2011-12-08

An Integrated Geophysical and Geologic Study of the Paleogene-Age Volcanic Body and Possible Landslide Deposit on the South Slope of the Traverse Mountains, Utah

John C. Hoopes
Brigham Young University - Provo

An Integrated Geophysical and Geologic Study of the Paleogene-age Volcanic Body and Possible Landslide Deposit on the South Slope of the Traverse Mountains, Utah

John C. Hoopes

A thesis submitted to the faculty of
Brigham Young University
in partial fulfillment of the requirements for the degree of

Master of Science

Department of Geological Sciences

Brigham Young University

December 2011

John H. McBride, Chair
Eric H. Christiansen
Bart J. Kowallis

ABSTRACT

An Integrated Geophysical and Geologic Study of the Paleogene-age Volcanic Body and Possible Landslide Deposit on the South Slope of the Traverse Mountains, Utah

John C. Hoopes
Department of Geological Sciences
Master of Science

Development of homes, roads, and commercial buildings in northern Utah has grown significantly during the last several decades. Construction has expanded from the valley floor to higher elevations of benches, foothills, and other elevated regions of the Wasatch Mountain Front. Construction in the higher elevation areas are a concern due to potential for landslides, both new and reactivated. Landslides have been identified in this region and are dated as Pleistocene to historical in age. A possible landslide of about 0.5 km^2 on the south slope of Traverse Mountain has been mapped by the Utah Geological Survey in 2005. Its surface exhibits hummocky topography and is comprised of Oligocene-age volcanic ash, block and ash flow tuffs, and andesite lava. Landslides along the Wasatch Mountain Front are complex features usually characterized by dense vegetation and poor outcrop and require a combination geological and geophysical methods to study their thickness, slope, lateral extent, and style of emplacement. Our study incorporates trenching, boreholes, and LiDAR aerial imagery. Unique to the study of landslides is our use of seismic reflection with a vibroseis source over the mapped landslide deposit. The seismic parameters of source, station spacing, and processing method provide a coherent, albeit low-resolution, image of the upper 500 m of the subsurface beneath the landslide. A major reflector boundary in our seismic profiles has an apparent dip of 4° to the south, approximately parallel with the surface topography. Its elevation and seismic character are indicative of a contact between the Oligocene-age volcanic rocks on top of a portion of the Pennsylvanian-age Bingham Mine Formation, a mixed carbonate and siliciclastic sequence. The reflector defines an asymmetric graben-like structure bounded by a north-northwest-trending normal fault system. Analysis of trenches, boreholes and local geology reveals a faulted, chaotic body of block and ash flow tuffs, surrounded by andesite lavas. Using LiDAR and surface geological reconnaissance, a possible toe or margin of a landslide has been interpreted in the north-west portion of the study area. The combination weakened block and ash flow tuffs and abundant clay production from this unit contribute to the likelihood of a coalescence of landslides in this mapped landslide area. The integration of LiDAR, trenching, boreholes and reflection seismology provides the range and resolution of data needed to assess the complex geology of landslides.

Keywords: Traverse Mountains, Utah, landslides, geophysics, Tertiary, Paleogene, Eocene, Oligocene, volcanic, andesite, block and ash flow tuff, andesite, 2D seismic, reflection seismology, vibroseis, boreholes, trench, LiDAR

ACKNOWLEGMENTS

I would like to thank my wife and family for their support as I've been a student the last several years at Brigham Young University. I also give equal thanks to my mentor, John McBride and my committee, Eric Christiansen and Bart Kowallis, for their support and efforts in all phases of this project. Software grants to Brigham Young University from the Landmark (Halliburton) University Grant Program (ProMAX2D™) and from Seismic Micro-Technology (The Kingdom Suite™) made the seismic processing and interpretation possible. I also thank Geostrata LLC for data (borehole, trench and LiDAR) and access to the study area which made the bulk of the surface geologic interpretation possible.

Table of Contents

Figures

Introduction

Landslides have become a growing concern along the Wasatch Mountain Front of northern Utah. Millions of dollars are spent annually in the study and hazard mitigation of landslides, debris flows, and rock falls along the Wasatch Mountain Front every year (Ashland and Christenson, 2007). This study is designed to evaluate the dimensions and kinematics of a mapped (possible) landslide near an area of recent home development on the south slope of the Traverse Mountains near Draper, Utah (Figures 1 and 2). The study is unique in methodology as it integrates information from trenches, boreholes, LiDAR and a vibroseis seismic reflection surveys.

Sixty one percent of Utah's population resides in a geographically small area comprising the cities and suburbs of Provo, Salt Lake and Ogden (Census Bureau, 2009; Visitor Center, 2010). Population growth has influenced the construction of houses and other structures in close proximity to mountain front terraces, foothills, and other elevated topography of the Wasatch Mountain Front. In these areas of higher elevation and steeper slopes, landslide susceptibility and hazard tend to increase. Higher elevation slopes generally have increased precipitation, and may be more prone to water table fluctuations and sliding in the spring months (Ashland, 2009). The wettest year recorded in Utah (1983) produced one of the largest landslide-related disasters in the U.S. The Thistle Landslide, 16 miles (10 km) east of Spanish Fork, dammed a river, flooded a small town, and interrupted a major highway and rail system. The total cost of damage was several hundred million dollars, the most economically damaging landslide in U.S. history (University of Utah, 1984).

Landslides, debris flows, rock slides, and falls have all been documented and studied in Utah (Elliot and Kirschbaum, 2007). These movements and failures share some common

characteristics. Bogoslovsky and Ogilvy (1977, p. 562) describe any of these movements as the "sudden or gradual rupture of rocks and their movement down-slope by the force of gravity". This is commonly facilitated by a two-step process where the rocks and soils are first weakened over time and then "triggered" to move under the force of gravity until they re-stabilize (Griffiths, 1999). This usually produces a scarp, or vertically displaced separation from the bedrock in the higher elevation of the slide, a glide plane, or basal surface which separates the moving mass on top of the bedrock and a toe or accumulation of the moved material.

Evaluation of a landslide's size, slope, thickness, mechanical stability, and history of movement all contribute to minimize risks where structures and other construction are planned. Both invasive and non-invasive methods can be used jointly to study the dimensions of landslides. Geophysical methods have proven successful in understanding the structure, and a variety of mechanical characteristics of landslides (Bláha, 2009; Bordoni et al., 2007; Tingey et al., 2007; Williams and Pratt, 1996). In conditions of restricted budget and environmental concerns, non-invasive methods may be preferred.

Surrounding the study area (Figure 3) are residential zones and roads built since the early 2000's. The primary leading goal of this study is to evaluate the use of integrating disparate geological and geophysical techniques for assessing landslide characteristics for an undeveloped portion of the Traverse Mountains. Primary objectives of this study are to identify and describe the possible landslide slip surface (glide plane), deposit thickness, and effectiveness of the methods used. Secondary objectives are to provide interpretations for the study area's geologic history and cause of landslide activity. This study also provides a case history that can serve as a model for how to integrate different data sets and strategies for studying landslide-prone areas.

Geological Setting of the Study Area

The Traverse Mountains are a salient of the Wasatch Mountains in northern Utah (Figure 1). Deviating from the fairly consistent north-south Wasatch Mountains, the Traverse Mountains more or less follow an east-west orientation. The (western) Traverse Mountains cover about 50 square kilometers and have a maximum elevation of 1645 m (5400 ft above sea level, Figures 2 and 3). The westernmost portion is near the main transportation corridor of Interstate 15, connecting most major cities in Utah. The study area is located on the south slope of the Traverse Mountains near areas of residential and commercial developments (Figures 2, 3 and 4).

The Traverse Mountains have been influenced by four distinct episodes of geologic development (Biek, 2005b). The bulk of the mountain's interior has been interpreted to be comprised of an upper member of the Pennsylvanian-age Oquirrh Group called the Bingham Mine Formation. This mixed siliciclastic and limestone sequence was deposited in a shallow sea and may have accumulated more than 15,000 feet (4571 m) of sediment (Tooker and Roberts, 1970). Based on outcrop similarities of the north and west sides of the Traverse Mountains (Biek 2005a), this unit has been interpreted to extend throughout the subsurface of the mountain complex. Small outcrops near the study area have been interpreted to likely be from the Bingham Mine Formation, which consists locally of fractured orthoquartizite and sandy limestone fragments (Biek, 2005a).

The second phase of the Traverse Mountains' geology is marked by Oligocene volcanic activity. Between about 40 and 20 Ma, rhyolitic, andesitic, and ash flow eruptions were wide spread across portions of western Utah and most of Nevada (Best and Christiansen, 1991; Miller and Gans, 1989). Thick igneous sequences of intermediate composition volcanic and volcaniclastic rocks, erupted through and covered the Bingham Mine Formation strata.

Geochemical analysis found the majority of the Traverse Mountain volcanic rocks to be approximately 35 Ma old (Biek, 2005a). The majority of the rocks found within the study area are andesite lavas and block and ash flow tuffs from this time period.

The third geologic phase is associated with the extension of the Basin and Range province. The Traverse Mountains are cut by normal faults striking in several orientations, confirmed as early as the 1940s when a 4.5 km long subsurface aqueduct, approximately 2.5 km east of the study area, was constructed through the Oligocene volcanic sequence between the cities of Alpine and Draper (Murphy and Gwynn, 1979), and more recently by surface mapping (Biek, 2005a and b). The Fort Canyon fault (Figure 2) in the northeast edge of the Traverse Mountains links the mostly north-south trending Salt Lake and Provo segments of the Wasatch Fault system (Bruhn et al., 1987). Our study area is in close proximity to several notable faults that represent a variety of extensional episodes not necessarily restricted to the onset of Basin and Range extension (Biek, 2005a). Closest to the study area are normal faults, striking mostly north-south and east-west on the western and southern margins respectively (Figure 3).

The final phase of the development of Traverse Mountains includes alluvial fan deposition, soil development and landsliding. Since the Oligocene, alluvial fans were created by erosion of the Pennsylvanian and Oligocene volcanic rocks along steep slopes. Lacustrine sediments were deposited by Lake Bonneville more recently, about 14.5 ka ago. The alluvial and lacustrine deposits are common in the lower elevations of the Traverse and Wasatch Mountains outside of the study area (Figure 2 and 3).

Landslides found at the Traverse Mountains are considered to be Pleistocene to historical in age (Biek, 2005a; Tingey et al., 2007). These features are mapped as either ‘old’ or ‘young’ (Biek, 2005a) based on how surface morphology contrasts with adjacent autochthonous rock.

The mapped landslide within our study area is considered to be old because of the greater development of drainages and their increased depth of incision. The surface and topographic texture of the surrounding Oligocene rock is considered to be autochthonous and has a subdued contrast because it has endured a longer period of weathering compared to 'young' landslides (Biek, 2005a, Figure 3). The Little Valley landslide studied by Tingey et al. (2007) to the north west of our study area is considered young and has more obvious landslide morphology: less incised drainages, more sag ponds, and a glide surface identified from subsurface data (Tingey et al., 2007).

Access to the Oligocene and Pennsylvanian rock unit outcrops is difficult for our study area since the Traverse Mountains are covered by soil and dense vegetation (Figure 4). The interpretation of geologic units is based on a few outcrops and surface debris that later has been observed in excavated trenches (1-3 m deep, Figure 5a). In most locations, the immediate subsurface is a dark, organic rich soil (commonly referred to as the 'A horizon') followed by a less organic rich 'B horizon' (Figure 6). Both have volcanic rock fragments increasing with depth to more massive block and ash flow tuffs or andesite lavas 2-3 m below the ground surface.

Volcanic rocks in the study area are primarily block and ash flow tuffs and andesite lavas with varied amounts of fracturing and degrees of hydrothermal alteration. Ash and block and ash flow tuffs usually contain suspended fragments of andesite lava (pebble to boulder sized) in their matrices (Figure 7). Intact fabrics of these tuffs are commonly dipping southward, similar to those volcanic bodies in the east Traverse Mountains documented during the aqueduct tunnel construction (Murphy and Gwynn, 1979). Andesite lavas are black to reddish brown in color and vary to boulder and horizontal configurations (Figure 8). The range of hydrothermal

alteration of the block and ash flow tuffs and andesite lavas ranges from durable, hard and preserved minerals (euhedral biotite and hornblende) and pumice to friable, sand and clay consistencies.

Methods

Assessment of method accuracy

In order to maximize the effectiveness of this study, a variety of geological and geophysical methods were used to sample different depths and properties of the subsurface, including trench, borehole, LiDAR, seismic reflection, surface reconnaissance, and previous geological surface mapping (Figures 5a and 5b). The seismic data were acquired by Brigham Young University. Trench, borehole and LiDAR data were gathered by other groups and were not always consistent in notation, descriptions and interpretations. Several meetings took place with the Utah state geologists who mapped the study area or had experience mapping landslides in Utah. Meetings also took place with Geostrata LLC who oversaw the geotechnical evaluations (boreholes and trenches) in order to discuss their methods and any needed corrections to the data sets made available to us.

Trenches

The trenches provided 2D profiles for the analysis of near-surface geology. Their walls exposed soil types, structural deformation, clay content, and features associated with possible landsliding of Oligocene age volcanic rocks. The trenches cover a large portion of the study area and some regions outside of it (Figure 5a). Locations for trenching were selected by Geostrata LLC in order to sample both the mapped landslide (allochthonous) and undisturbed (autochthonous) portions of the Oligocene volcanic rocks. Together with the boreholes, the trenches provide control of the upper-most subsurface geology where the seismic reflection survey cannot provide information.

Heavy construction excavators dug trenches between 2 and 3m deep by 2 to 3 m wide for various lengths (several 10s m to 100s m). The trenches all follow an approximate north to south, down-slope orientation. This was in order to provide a cross sectional view of any downslope movement that may have accompanied landslide activity. After excavation, the trench walls were scraped smooth to allow for more accurate observations (Figures 5a, 6, 7, and 8). High-resolution sketches (scale, 1 in : 4 ft horizontal) were made of the interior walls along with lithologic descriptions and structural feature notes. The sketches were augmented by digital photography of the logged trench walls.

Boreholes

Thirteen locations for boreholes were selected by Geostrata LLC on the south slope of the Traverse Mountains in order to sample most of the mapped landslide and to provide samples of the deeper subsurface. Boreholes were drilled with both conventional rotary coring and sonic drill devices. Conventional or rotary coring was abandoned due to the poor consolidation of rock intervals encountered and inability to collect the cored rock. The sonic drill rig used a vertical pipe vibrated at high frequency to penetrate the ground, which also brought the cuttings to the surface. For every 2 to 4 ft (~1 m) drilling interval, the cuttings were brought up to the surface, described, and stored in elongate sample bags. The extracted cuttings typically had the consistency of gravel fragments. The drill rig penetrated anywhere between 30 to a maximum of 90 m (100 to ~300 ft).

LiDAR

LiDAR (Light Detection and Ranging) data were acquired via a small aircraft flying over the Traverse Mountains (Tingey et al., 2007). Our analysis uses a version of these data that attempts to filter out vegetation and buildings called 'second return' LiDAR. This second return data set is estimated to have a resolution of 0.8 m (~2 ft) and can show details of surface morphology and ground texture otherwise not visible in conventional aerial photography (Van Den Eeckhaut et al., 2006). The LiDAR mapping of the Traverse Mountains is intended to reveal textural variations and morphology of landslides while being able to spatially reference trench, borehole and seismic survey locations (Figures 5a and 5b). The working data set for our study is a mosaic of nine separate blocks compiled into a digital elevation model (DEM) using ArcGIS. A hillshade with a Z factor of 0.33 has been applied, with illumination orientations of N60°E and an attitude of 80° from the horizon (Figure 5b).

Seismic Reflection Profiles

Acquisition

The seismic survey array was positioned to image portions of the mapped landslide and underlying bedrock and immediately adjacent areas thought to be undisturbed rocks (i.e., autochthonous). The overall survey design consists of a long two-dimensional (2D) "dip" profile oriented downslope with three auxiliary cross ("strike") lines to help provide some 2.5D control. An Industrial Vehicles International (IVI) Envirovibe™ (vibroseis) source was used along pre-existing and recently bull-dozed dirt roads (Figure 5a and 9). The profiles were recorded using 28-Hz geophones with a receiver and source spacing of ~3.05 m (10 ft) with a lateral source-receiver offset usually of about 2 m (6 ft, Figure 9). The vibration generated a 20 to 160 Hz

sweep, which lasted 12 seconds (s), and included a 3 s listening period for a total of 15 s per record. Three records were usually generated at each station, to be stacked during processing in order to enhance the signal-to-noise ratio.

The receiver array consisted of 120 or 96 channels, depending on the total length of the line. During the recording period, all channels were kept open which gave an asymmetric split in records. The nominal CMP (common mid-point) fold of cover was 48 or 60 on shorter cross lines and a maximum of 85 on line 1. The split spread of the array also provided partially reversed profiles that could be used for two-layer classical refraction static analysis based on direct arrivals and head waves (critically refracted waves). Recordings were made, uncorellated, with a 2 ms sample rate, but were displayed and monitored during acquisition with vibroseis cross-correlation for quality control purposes. Efforts were undertaken to minimize noise contamination by observing the changing weather, vehicles operating nearby, replacement of faulty geophones, and operating with an active noise monitor during the recording.

Processing

On-ground reconnaissance of the Traverse Mountains study area revealed a hummocky and irregular surface with variations in near-surface geology, soil type, and vegetation. Initial examination of the trench and borehole data confirmed a geologically heterogeneous subsurface that would present a challenging environment for seismic imaging. In order to refine the final image derived on the CMP stacked section, several of the data processing steps were experimental, including frequency filtering, refraction static modeling, and low-apparent velocity noise filtering (Figures 10 and 11).

A vibroseis cross-correlation was first applied to each field record using a synthetic sweep generated from 20 to 160 Hz. Each record was then examined for bad traces, which were eliminated from further processing, prior to stacking of the shot records (Figure 10). In preparation for deriving a shallow velocity model, first breaks of the shot records were chosen on the first positive excursion of the wave form following the direct arrival to the refracted wave. Using a two layer approximation for the shallow subsurface (i.e., a weathered zone overlying a higher velocity half space), we chose one direct arrival that intersected the headwave at the cross-over point that would be used in the refraction static modeling (Figure 11). In places the direct arrival-refractor interface was not clear and the diving behavior of the wave made cross-over points difficult to select.

We consider the use of a two-layer velocity model to be an approximation since the occurrence of diving waves implies a continuous increase in velocity as a function of depth. The approximate average velocities of the upper medium and primary refracting surface were 800 m/s and 2200 m/s respectively, based on measurements from shot records. A refraction static correction was then applied and a preliminary stacked section generated to estimate NMO (normal move-out) stacking velocities.

Before proceeding with further processing, a top mute was applied that eliminated the first breaks (direct arrivals and onset of headwaves or diving waves); however, it is likely that phases from the refracted waves and reflected waves are merged. The top mute was followed by testing different zero-phase bandpass (Ormsby) frequency filters applied in the shot domain, with a final choice of 15-25-150-200 Hz. The application of the frequency filter was preceded by a predictive deconvolution (120 ms operator length, 10 ms prediction distance), in order to reduce reverberation and shorten the waveform (Figure 12). An automatic gain control (200-ms

window) was necessary in order to reduce the effects of noise and to balance amplitudes. NMO velocity analysis was performed for each seismic profile and focused on the high-velocity reflectors that represent the top of the first significant rigid subsurface layer, resulting in a two-dimensional stacking velocity function (space and time varying). A second first-break muting was also accomplished just after CMP sorting and before stacking by applying a 30% stretch mute (any sample time-shifted over 30% is zeroed). Post-stack processing included a low-apparent velocity filter to remove the effects of scattering and a phase-shift time migration (constant velocity of 900 m/s). The final data stacks were initially converted to depth using the replacement velocity function associated with the static solution shifted to match the topographic datum (2000 m). Because the replacement velocity represents the velocity of a relatively shallow rigid layer that does not include the effects of the weathered zone and unknown deeper velocity inversions, these depth-converted sections likely indicate a maximum depth value for reflectors. A 2D RMS (root-mean-square) velocity model was derived from the NMO velocity analysis. Using the RMS velocity function shifts the primary reflector observed on the sections (see discussion below) an average of 70 m higher in elevation compared to using the replacement velocity for depth conversion. The final step was to correlate the cross ("strike") profiles with the one long north-south ("dip") profile in preparation for interpretation.

Interpretation Strategy

Interpretation of the seismic profiles was performed using a specialized seismic data interpretation software package where spatial data could be integrated (e.g., LiDAR and geologic maps). Both topographic elevation and isochore maps were generated from the reflection profile data. The focus of the interpretation is on the first rigid boundary, manifested on the CMP

stacked sections as a thin, multi-cycle reflection sequence. The disrupted nature of the laterally discontinuous shallow sequence above this boundary, consisting of ash and boulders, could act as point-source scatters. Thus the shallow sequence above the rigid boundary would be expected to attenuate the vibroseis signal especially at higher frequencies. Furthermore, the effective fold of cover is reduced in the shallow section above the first strong boundary. In the final processed stack, the first major positive excursion of the reflector series was not laterally continuous, and if used as the primary surface for interpretation, would have resulted in an inaccurate depiction of this horizon. Therefore, the second more continuous and coherent portion was chosen for interpretation below the primary onset of reflectivity (Figure 12). The surface we have interpreted then may be in places as much as about 15-20 m (~50-65 ft) below the inferred top of the actual reflective boundary. This interpretation strategy is similar to that used by other vibroseis seismic data sets recently collected along the Wasatch Mountain Front (McBride et al., 2008, 2010; Stephenson et al., 2011).

Results

LiDAR

The processing and mosaic construction of the high resolution LiDAR helped reveal surface and morphological details otherwise difficult to see because of terrain, vegetation cover, and accessibility. This level of resolution however includes some noise from the filtering out of vegetation and structures and when examined closely, there is some unnatural texture from processing and over correction. The general morphology of the surrounding Oligocene volcanic rocks and Biek's (2005a) mapped landslide can be described as hilly topography, extending from the base of artificial landfill to the north, and bordered on the east and west margins by south, south east trending drainages (Figures 3, 5a and 5b). However, the mapped landslide does appear independent of the surrounding volcanic rocks as it's separated by incised drainages on the west and east margins. The southern portion of the study area gradually transitions to a less steep hilly topography met by a flattened area developed for housing. The west and east drainages bordering Biek's (2005b) landside, are elongate with some small tributary drainages connected to them (Figure 8a and 8b).

Trenches

The trenches of the south slope reveal fractures, hydrothermal alteration, and structural variation of the Oligocene-age volcanic rocks. Most trenches contain the two volcanic rocks prevalent throughout the Traverse Mountains' south slope: andesite lava and block and ash flow tuffs. Andesite lavas varied in color and structural condition. Most were dark grey to reddish brown with fractures in all orientations. In some instances they were fractured internally while the matrix of ash tuff was intact. The majority of andesite lavas were resistant and difficult for

the excavator to penetrate, but some portions of the lava and blocks of andesite within the ash flow tuffs were hydrothermally altered, friable, and included clay-filled fractures.

Block and ash flow tuffs varied in its level of durability, fracture density of quantity of andesite inclusions. Portions of the ash flow tuffs are hydrothermally altered, which has left friable and clay-rich bands in irregular patterns. Texturally the block and ash flow tuffs were commonly friable with intervals of massive, more welded and unaltered ash. Boundaries between individual block and ash flow tuffs are usually very thin, marked with clay filled fractures. Occasionally, individual flows were distinguishable by contrasting color (light tan and brown to dark grey).

Trench DT-7 contains much of the geology generally observed in the upper 2-3 meters of other trenches throughout the study area (Figure 13). This trench also contains significant structural features not seen in the other trenches of the study area. The following paragraphs will outline a central portion of the trench, facing the western wall, and progressively describe the interior northward (from 320 ft to 720 ft markers). Location markers within the trench are given as distance in feet from the southern end. Orientations of fractures and faults are by extrapolated to the opposite side of the trench. This represents an approximation of these orientations and may vary regionally as we can only measure small portions projected across trench walls.

Soil layers are exposed in the upper 0.5-1.5 m of trench DT-7 (Figure 6). The upper layer, referred to as the “A horizon” (1-1.5 m thick), is more organic-rich and darker in color (Figure 13). The “B horizon” is about the same thickness, tan, less organic-rich but with more weathered ash and andesite fragments. In most cases, the Oligocene-age volcanic rocks (either the andesite lavas or block and ash flow tuff) are directly beneath the soil layers (~0.5-1.5 m

below surface). At 340 ft (104 m) the lithology is an interval of subangular and angular (2-8 cm) andesite and opalite fragments (Figure 13), stratified horizontally. Andesite particles are found lower in the trench and the opalite particles reside in the upper portion of the alluvium, which is approximately 30 m wide.

Within this same interval (340-370 ft from south end), the trench crosses a normal fault striking north-west and dipping about 44° northeast (350 ft or 107 m from south end – Figure 13). The fault plane does not propagate past the soil intervals and thus constrains the age to pre-soil development in this part of the study area. Overall offset is not measured due to the limitation of trench depth, but the smaller offsets are 10's of cm to half meter in displacement. This location of the fault in the trench corresponds to the topographic drainage of the western margin of the mapped landslide crossed by the profile (Figures 5a and 14). The fault zone, along with the overlying sediment fill, truncates against another block and ash flow tuff (440 ft or 134 m). At this contact with the block and ash flow tuff, we interpret a shallow normal fault dipping southwest, which structurally truncates the tuff against the alluvial fill (Figures 13 and 14).

At 452 ft (138 m) from the southern end, the block and ash flow tuff matrix has assorted andesite fragments ranging from 0.1 to 1.5 m in diameter. These are somewhat larger than those found in the previously mentioned block and ash flow tuff near the southernmost end of the trench which had gravel to some cobble sized fragments. Some tangential contact exists among the fragments, but they are mostly suspended within the ash matrix. This portion becomes progressively denser with andesite inclusions and tangential contact between markers 470-560 ft (143-170 m). At marker 554 ft (170m), a thick blue-white colored clay, with bands of red-yellow streaks, has imbricated wedges of distinct material (~0.5-1 m thick). This clay-rich band

curves from the ‘A soil’ horizon, down and to the north (554-584 ft or 169-178 m) and disappears beneath the base of the trench.

Directly north of the stacked clay band, the trench lithology is ash-rich, with occasional suspended andesite fragments. Above this ash-rich layer, a white clay resides just below the thin “A” soil horizon, and exhibits a systematically fractured (vertical and horizontally orthogonal) mosaic pattern (Figure 13). This clay extends from the 588 to 720 ft (180 – 219 m) markers, increasing from about 0.5 to 2.5 m thick where it terminates abruptly against several large, internally fractured bodies of andesite boulders. Over this same interval, the ash layer below becomes progressively thinner (~0.5-1 m) with some near-vertical fractures propagating through it and the white clay above. Some fragments of andesite at this interval are also offset by the fracturing. The white, systematically fractured clay is seen again at the 736 ft marker and continues to the north end of the trench (230.5 m).

Other trenches throughout the study area contain much of the geology observed in DT-7 with some exceptions. Pull-apart or transverse fractures are observed in trenches UNK-1 and DT-4 with approximate east-west mode one fractures (Figure 15). The gashes of tension fractures are filled with the less mature ‘B horizon’ soil, in which portions of the block and ash flow tuff matrix are suspended (Figure 15). In the trench cross-sectional view, the fractures have 1 to 10s of cm separation, opening voids oriented approximately east to west with little or no vertical displacement.

Approximately 80 m south of the south end of trench DT-11 a dike with a matrix of pebble or rich in gravel sized inclusions strikes approximately N65°E (Figure 5a). This silicified, durable to very weathered greenish colored vein is mostly vertical, cutting across all

other rocks in the trenches in which it is observed (DT-9 and the small test pit south of DT-11). The matrix of the dike includes angular and sub-rounded fragments of quartzite, andesite and pockets of opalization. Where it contacts the A and B soil horizons, it is weathered to a near clay consistency. Surface debris and in situ portions of the dike are cobble to boulder sized and have an approximately linear trend in the south western portion of the study area. The dike is relatively small in trench DT-9, and no surface fragments are seen in this part of the study area.

Boreholes

Boreholes provided critical information of the lithologic character below the surface many 10s of m beyond the range of trenches (approximately 30-90 m below the ground surface). The majority of the rocks encountered in the boreholes are categorized into two main types: block and ash flow tuffs and andesite lavas. Boreholes commonly penetrated one of these two rock types with thicknesses ranging from 1 to 10 m.

Cuttings recovered from the boreholes varied in degree of hydrothermal alteration, clay content, fracture density, and durability. Figure 16a illustrates a generalized log of the lithologies observed among the 13 boreholes in the study area. Intervals that have higher clay content and are structurally weaker are interpreted to be hydrothermally altered. Durability ranged from massive or without many fractures to zones of high fracture density and increased friability. Intervals with more alteration would produce cuttings with clay-filled fractures, which was not an effect of drilling. In 3 boreholes, multiple water tables were encountered and ranged between approximately 50 to 200 ft below the ground surface without a consistent depth between the holes.

The depth of hydrothermal alteration did not follow any pattern in the boreholes (Figure 16a and 16b). The grade of hydrothermal alteration would progressively increase or decrease with depth in intervals ranging from one to tens of meters in both andesite lavas and block and ash flow tuffs. Most boreholes (DB-1, DB-2, CB-1, LB-6, LB-7, LB-10, LB-13, and LB-15) were terminated at an interval of massive andesite that was minimally altered andesite approximately 50 m below ground surface. Other boreholes (LB-4, LB-11, LB-12, and LB-14) were terminated in more hydrothermally altered and fractured andesite at approximately 65 m below the ground surface (Figure 16b). The drilling range, time, and economic costs of the project did not allow for drilling to greater depths.

Five of the 13 boreholes were noted to have a pattern consisting of block and ash flow tuff on top of andesite lava, being the last rock type encountered in the borehole (Figure 16b). These boreholes are in the northern portion of the mapped landslide deposit. The thickness of these block and ash flow tuffs ranged between approximately 55 and 255 ft (17-78 m). The other eight boreholes penetrated thin 2-5 m thick layers of block and ash flow tuffs on top of andesite lava. The block and ash flow tuff bodies have chaotic, smaller intervals of more resistant ash and andesite lava inclusions. In both andesite lava and block and ash flow tuff lithologies, clay-rich zones are found at all depths of the boreholes. Zones of increased water or moisture content are commonly found just above the more clay-rich intervals of both andesite lava and block and ash flow tuff.

Seismic Reflection Profiles

Due to the low-frequency character of the vibroseis source, the seismic reflection CMP stacked sections have limited resolving power. The dominant frequency of the coherent signal is

about 35 Hz within a source frequency bandwidth of 20-160 Hz. Using the Rayleigh criterion, we estimate the vertical resolution to be about 16 m (assuming a velocity of 2200 m/s). In other words, to actually measure the offset of a surface (i.e. faulting), it must have least 16 m of offset. The detection limit of a vertical offset is estimated to be 8 m (one eighth wavelength rule).

Two versions of the depth-converted CMP sections were derived from the 2.7 km of 2D seismic profiles processed. The replacement velocity of 2200 m/s offers a conservative depth (deeper) of the basal reflector (Figures 11 and 17). This version is considered conservative in the sense that a thicker mass of material that could potentially be mobilized as part of a landslide mass would increase the landslide hazard. The RMS velocity model offers a less conservative or shallower estimate for the basal reflector. RMS velocity modeling takes into account the averaging of high- and low-velocity zones instead of assuming a uniformly constant (i.e., replacement) velocity (Figure 11). Having observed such a heterogeneous body of rock in the trenches and boreholes, the RMS velocity model likely provides a more accurate assessment of the reflector's depth.

"Dip" Line 1

Dip line 1 has a total length of about 1371 m (CMP coverage) and extends through the main corridor of the mapped landside deposit (Figure 8b). The coverage provided by line 1, when augmented with several cross lines, follows the suggestion by Bogoslovsky and Ogilvy (1977) to place survey lines parallel and perpendicular to the axis of landslide flow direction. The combination of several seismic profiles in this configuration helps to approximate a subsurface model and compare differences in lithology within and outside the mapped landslide.

We consider line 1 to be of the best quality since it has a greater length and high fold of cover (maximum of 85) compared to the other four lines and provides the best opportunities for interpretation. This line shows a major, laterally persistent reflector throughout the length of profile (Figure 17). In map view, the interval between the ground surface and reflector does not show a uniform thickening or thinning trend, but has two isolated areas of slightly greater thickness (Figures 18 and 19). The depth to reflector (using the RMS velocity conversion) is on average 90 m (ranging from 105-75 m) below the ground surface. The slope of this reflector dips southward approximately 4° from horizontal (7 % grade, based on the conservative depth conversion) slightly less than the approximate slope of the ground surface above (6-7° or 11% grade). The basal reflector has some topographic highs and lows but trends relatively parallel to the ground surface. At finer scales, the match is not one-to-one. Some flat areas of the reflector correspond to dipping segments of the ground surface (e.g., CMP 650-750, 800-900). Some breaks in the seismic profile or discontinuous events, may signal the presence of faults, but do not appear to have major vertical displacements. It is possible that minor variations in the reflector structure may be a consequence of inaccurate first break (direct and refracted arrival) picks that affected the refraction statics model.

"Strike" Lines

Four strike CMP profiles were collected (Figure 5a, lines 7, 8, 9, 10, respectively with CMP coverages of 509 m, 288 m, 323 m, and 389 m respectively). Since the refraction statics solution for the individual lines did not cover the exact same range of velocities and offsets, the final processed lines would be expected to be somewhat offset relative to dip line 1. Seismic correlation was made between dip line 1 and the three strike lines (7, 8, and 9) by matching the

same positive excursion to line 1 (Figures 12 and 17). Some manual adjustments to elevation were made to the strike lines to improve the match. Cross lines 7, 8, 9, and 10, although much shorter than line 1, help to constrain the 3D geometry of the basal reflection observed in line 1. These strike lines show the same reflector character as seen on line 1 at the same depth when correlated. Line 8 is somewhat anomalous in that it does not correlate well with line 1. It may be that its profile is on the edge of a discontinuity or fault where it intersects line 1.

The strike lines 7 and 8 show a slightly curved or basin-like surface for the basal reflector, whereas lines 9 and 10 are somewhat more planar (Figure 17). The upward curving of the edges is judged to not be an over-migration artifact since the unmigrated sections also show this effect. In map view, south of line 8, the contoured surface of the basal reflector displays an elongate portion extending north, north-west (Figure 19). In the north-eastern portion of the study area, the elevation of the basal reflector rises more rapidly than in the west, forming an asymmetric graben. Towards the southern end of the seismic coverage, the basal reflector slopes downward to the south. In the isochore map produced for the ground surface-to-basal reflector interval (Figure 18), the volcanic deposit has two distinct zones of thickening, bordered by areas of lesser thickness. In figure 18 we note that line 9 marks a thin zone between two thicker bodies north of line 7 and south of line 9.

Discussion

The integration of multiple geological and geophysical methods is necessary when studying landslides and their complex geomorphological and subsurface characteristics (Bruno and Marillier, 2000; Jongmans and Garambois, 2007; McCann and Foster, 1990). The utilization of LiDAR, trenches, boreholes, and exploration seismology all provide varied ranges of depth and geological resolution. The following will provide our integrated interpretations of the surface and subsurface data sets.

Surface geologic interpretation

LiDAR and Aerial Photography

LiDAR is an effective method of mapping relatively young landslides, based on subtle surface character variations. In our analysis of the LiDAR expression of the surface topography of the study area compared with aerial photography and, we note a lack of textural contrast between the landslide as mapped by Biek (2005a) and the surrounding ground surface (Figures 5a and 5b). The older age (relative to known younger landslides in the area - e.g., Tingey et al., 2007) of the landslide surface appears to be related to increased weathering time and has accordingly lost the more obvious hummocky landslide texture observed in younger landslides. As the mapped landslide appears to be relatively old, it is anticipated that textural variation would be subdued compared to the surrounding Oligocene-age rocks. The topographic patterns viewed with aerial photography and LiDAR display elongate drainages on the west and eastern margins (Figures 3 and 5b). Drainages are one of the main features used with LiDAR mapping to separate landslide masses from autochthonous rocks. Biek's (2005a) landslide is constrained on the east and west by drainages trending north-south (Figure 5a and 5b). In most cases, the

margin separating landslides and autochthonous surfaces becomes a drainage or linear depression at the surface (Van Den Eeckhaut et al., 2007). In trench DT-7, the margin of a landslide is defined by a drainage separating the mapped landslide and Oligocene-age volcanic rocks (Figures 13 and14). In our study area however, drainages, gullies, and topographic variations do not always correlate to landslide boundaries as detected in a trench. For example, trenches DT-12a and DT-12b were excavated across a drainage between the mapped landslide and Oligocene-age volcanic rocks (Figures 5a and 5b), but showed little variation in the exposed rock relative to the marked variations in trench DT-7. We therefore cannot assume that all drainages act as reliable indicators of lithologic boundaries of landslide features in the study area.

Boreholes and Trenches

Figure 16 models the borehole and trench lithology classified by most prevalent rock type. Those trenches and boreholes containing about 70% or more of either andesite lava or block and ash flow tuff are representative of the entire study area. When correlated, the borehole and trench profiles reveal a corridor of block and ash flow tuff within the middle of the study area approximately 200-350 m wide (Figures 16a, 16b and 21). The long axis of the block and ash flow tuff unit is oriented approximately down-slope parallel with the hillside slope (Figures 20, 21 and 22). The borehole and trench profiles indicate that the block and ash flow tuff body has a foundation of andesite between 50-255 ft below the ground surface, east and west margins where borehole control is available (Figures 5a and 16b).

Within the block and ash flow tuff complex, fabrics and architecture are laterally discontinuous, truncating against smaller order block and ash flow tuffs, and vary in thickness

and hydrothermal alteration. Recent studies of relatively young block and ash flow tuffs on the Merapi volcano of Indonesia, exhibit this same architecture of block and ash flow tuffs coalescing and truncating against one another (Charbonnier and Gertisser, 2008). Figure 16b illustrates the complexity of the block and ash flow tuff body in a number of borehole profiles parallel to the likely flow direction. Ground penetrating radar surveys of the Merapi block and ash flow tuffs revealed progressive overlapping and truncation within the body as individual ash flow tuffs coalesced (Gomez et al., 2009). The thickness of these smaller order block and ash flow tuffs range from 2-3 to 8 m (Charbonnier and Gertisser, 2008), consistent with block and ash flow tuff thicknesses in the trench and borehole profiles of our study area.

Figure 22 provides a conceptual model of the internal structure of the block and ash flow tuff bodies. This cross section assumes that the block and ash flow tuff body has flowed approximately south, and has not been faulted or experienced landslide activity. Due to the spacing of boreholes and trenches, we are unable correlate individual block and ash flow tuffs and recognize its internal structure is likely more complicated than the model (Figures 16b and 22). The combination of landsliding and faulting of the block and ash flow tuff complex most likely creates overlap and or removes whole portions of the flow, further complicating its structure. The coalescence of small block and ash flow tuff lobes into a larger body would also explain the variability in borehole lithologic profiles. The block and ash flow tuff configuration follows the model described by Fisher and Heiken and their analyses of Mt. Pelée's eruption (1983). With the collapse of the lava dome(s), the ash and rock mixture is too heavy to be suspended in the air and flowed down-slope (southward). Like Mt Pelée, the erupted material in the study area likely followed a valley or collected in a topographically low region. With many small lobes stacked and truncated, there is a large diversity of hydrothermal fluid pathways and

potential for alteration. As fluids penetrated the block and ash flow tuffs, mineral alteration led to the development of clays prevalent in the study area. This model of development also accounts for the perching of water tables noted in boreholes throughout the study area.

Trench DT-7 contains significant structural features formed after the Oligocene volcanic activity. The normal fault striking through the drainage crossed by trench DT-7 (Figures 13 and 14 - 107 m from south end) establishes that tectonic extension has occurred along the western margin of the study area. It is important to note that the fault does not propagate to the surface, but is covered by alluvial sediments and is therefore no younger than Miocene or Pliocene in age. In trench DT-10 another normal fault with the same orientation, connects to the fault location seen in trench DT-7 by a northwest trending drainage. This suggests that the western margin of the study area is bounded by a normal fault trending northwest to southeast, with the hanging wall on the north-east (Figures 5a and 14). The fault may be longer since no other trenches cross this feature. The orientation of the DT-7 and DT-10 fault follows the trend of other faults identified by Biek (2005a) to the west with only a few degrees difference in strike (Figures 3, 5a, and 14).

Transverse fractures were identified in trenches DT-4 and UNK-1 (Figure 5a and 15). Fractures of this type are observed in landslide bodies when deformation pulls the ground surface apart as the subsurface deforms and moves (Mario, 2003). Had the landslide been more fluid and comprised of weaker soils, such fractures may not have been formed and preserved. As the landslide progresses, these fractures form within and around the margin of the landslide body. Though not recognized solely in landslides, transverse fractures represent extensional activity of the block and ash flow tuff (Zhang et al., 2002). According to Martel (2004), *en echelon* (open gash) fracture patterns can form at the flanks and crown of autochthonous bedrock located

outside the landslide mass. The fractures in trenches DT-4 and UNK-1 are within Biek's (2005a) mapped landslide and are therefore indicative of internal landslide deformation rather than deformation of peripheral bedrock (Figure 15).

One of the most crucial lithologic features of the study area is the thick, stacked clay shear bands observed in trench DT-7 (260ft / 80 m; Figure 13). This feature has two contrasting rock types on either side: to the south, a block and ash flow tuff and to the north, clay and sand sized particles. The clay band separating the two lithologies has a duplex structure verging from north to south over the volcanic unit. A focus of our investigation included zones of higher clay content because these are key in identifying glide surfaces. Shear planes or margins and toes of landslides are all products of mass movement where one body of rock or soil has moved over another. Sand-to-clay-sized particles are both a product and facilitating agent of landslide movement, increasing the clay content as the displacement of the landslide increases (Shuzui, 2009). Landslide margins and toes have been documented in the active Slumgullion landslide in Colorado (Mario, 2003). The advancement of the toe acts like a bulldozer in that the material is thrust over the older surfaces (inactive toes) repeatedly. We interpret the stacking of the clay bands in trench DT-7 to be an accumulation where a landslide toe or margin has been thrust over Oligocene-age rock in a southward direction (Figures 13 and 22). As this advancement has taken place, clay has been developed by basal friction of the landslide on the surface from which it separated and formed a duplex pattern as it moved over the ash flow tuff.

To classify the study area as a stationary mass (i.e., without landsliding), attention must be given to features that could correlate across (i.e., cross cut) the mapped landslide, and thus suggest that the mass has not moved (i.e., autochthonous). This cross cutting relationship depends on the generalization that landslides become chaotic masses as they move. However, a

mass under the influence of gravity may simply be translated along a surface with topographic reference points remaining in the same position relative to one another after movement. This possibility exists since Utah's landslide history has documented rock slides or translational landslide activity, although not as commonly as rotational or fluid (flow) type landslides (Elliott and Kirschbaum, 2007). The pebble dike observed in trenches DT-9, and in the small test pit south of trench DT-11 was taken to be a reference point for landslide activity. Some surface fragments of the dike are located between trench DT-9 and the test pit south of DT-11, but only over a distance several tens of meters south of DT-11. Had these fragments been consistently visible across the surface between these trenches in an unbroken line, a convincing case may have been made that the Oligocene dike has cut across rocks otherwise undisturbed (Biek 2005a). This would imply that no landslide movement has taken place to offset its position. However, since the dike observations cannot be firmly correlated across the landslide between the two trenches, what appears to be a single dike may represent just part of a swarm or cluster of dikes in the study area that follow a similar orientation (Figure 5a).

Geologic interpretation of the Seismic Survey

Reflection seismology has been successful in the identification of landslides and measuring their thickness and dimensions in a variety of geological settings (Bordoni et al., 2007; Bruno and Marillier, 2000; Glade et al., 2005). Surficial reconnaissance of the study area led us to pursue our seismic processing with the following model in mind: a chaotic, variable velocity medium of landslides or volcanic debris lying on top of rigid bedrock with more a

uniform seismic velocity. Depending on the seismic velocity model, the range of depths for the basal reflector is between 90 to 170 m below the ground surface (Figures 17, 19 and 20). However, in order to account for potential low-velocity zones within the Oligocene age volcanic rocks, we will assume the RMS velocity model is more representative of the volcanic material in the shallow subsurface. Assuming the RMS velocity model, we identify a strong reflector between 80-100 m below the ground surface across the study area (Figures 17, 19 and 20). This estimate is 20-30 m shallower than Biek's estimate of approximately 130 m below the ground surface (2005a – cross section B-B'). According to Biek (2005a), the lithology below Oligocene age volcanic rocks is the Pennsylvanian-age carbonate-siliciclastic sequence. As our depth-converted seismic shows a shallower depth, we can assume that it may be the Pennsylvanian-age rocks that are located somewhat closer to the surface than Biek's (2005a) estimate or a glide plane within the Oligocene volcanic rocks (Figure 20).

The long dip line 1 imaged the basal reflector as an undulating surface with a variable thickness of volcanic rock above it (Figures 18 and 19). Offsets or undulations may represent faults or possibly irregularities of the velocity field related to inaccuracies in the initial first break (direct arrival and headwave) picks used to model a velocity static correction. Regardless, the reflection is laterally consistent and represents a strong velocity contrast. The basal reflector, confirmed with the 2.5D control provided by cross lines 7, 8, 9 and 10, has an irregular topography not expected of an intact sediment sand sheet or carbonate platform (Figures 17 and 20). However, as indicated by the faulting that cuts across the study area and most of the surrounding mountain range, the south flank of the Traverse Mountains has experienced deformation prior to and during the Basin and Range extension. Therefore, faulting is likely at the depth of the basal reflector and possibly deeper. If this boundary is in fact the top of the

Pennsylvanian-age rocks, it may represent an erosional surface since the time between its deposition and Oligocene-age volcanic activity is over 200 Ma.

Faulting and structural variation of the basal reflector are difficult to interpret from a single dip line due to the expected 3D complexity of the interpreted landslide deposit. In cross lines 8 and 9 (Figures 17, 19, and 20), we interpret the depression or graben-like feature of the basal reflector as an expression of possible faulting. The north and north-west strike of faulting is similar to that shown by prior geological surface by Biek (2005a, Figures 3 and 5a). Figure 23 shows the orientation of the fault mapped with our observations in trenches (DT-7 and DT-10), and the interpreted seismic horizon. The topography of the reflector appears to be a slightly elongated graben extending to and possibly involving the displacement seen in seismic lines 8 and 9 at CMP locations 290, 340 and 325 respectively (Figures 17 and 23). At depth, the trend in offset of the basal reflector, projects to the surface approximately at the location of the fault interpreted from trenching (between trenches DT-7 and DT-10). In seismic line 8, there may also be an antithetic fault dipping westward, but it is not expressed in the trench profiles. Since the fault propagates through the Oligocene unit, its maximum age is late Oligocene, likely related to Basin and Range extension, prevalent in surrounding parts of the Wasatch and Traverse Mountains.

Addressing a landslide hypothesis for the south flank of the Traverse Mountains

An important factor to consider when identifying landslides are its dimensions (thickness and surface area). Numerous inventories worldwide of landslide dimensions show some trend in their area or lateral extent, correlating to their overall volume. The area of the landslide as it is

presently mapped by Biek (2005a) is approximately 0.5 km^2. If we assume a thickness of about 150-175m between the ground surface and basal reflector (using the replacement velocity to compute thickness) as all part of a landslide, its volume would be approximately 0.08 km^3. A less conservative estimate of about 80-100 m based on using an RMS velocity function shrinks the volume to approximately 0.05 km^3. The compiled landslide volume and area ratios by Kalderon-Asael et al., show that either thickness would fit the global trends in landslide volume vs. thickness (2008). As landslide area increases, thickness increases and therefore and overall volume tends to increase. Some lithologic similarities of our study area's volcanic rocks experiencing landslides resembles characteristics of the described by Moon and Simpson (2002). The mega failure identified in New Zealand's Coromandel Volcanic Zone, is comprised of extensively hydrothermally altered andesite, which produced a slide of about 400 m thick and a total volume of approximately 1 km^3. Although the mapped landslide in our study area is not as thick as the North Island New Zealand example, it establishes the possibility that when hydrothermally altered, andesite and block and ash flows are capable of massive catastrophic failures.

Based on the surface and subsurface observations, we propose the following geologic model for the mapped landslide on the south slope of Traverse Mountain. Following the deoposition of Pennsylvanian-age mixed carbonate and siliciclastic strata, this portion of the Traverse Mountains may have been a region pre-disposed to accumulate less viscous, block and ash flow tuffs during Oligocene volcanic activity. The coalescence of block and ash flow tuffs into our study area suggests paleo-topographyic valley or depression where flowing volcanic debris could have been concentrated. These same block and ash flow tuffs were then mechanically weakened by hydrothermal activity, which effectively increased their clay content

and potential for landsliding. Faults within the study area and along the western margin of the mapped landslide are most likely the result of Basin and Range extension (Biek, 2005a and b). Landsliding within the study area was made possible by the weakened of block and ash flow tuffs and possibly triggered by seismic activity.

We interpret the baseal reflector in our seismic profiles to be a glide surface within or near the base of the Oligocene-age volcanic rocks, possibly overlaying another separate series of block and ash flows or the Pennsylvanian-age carbonate- siliciclastic strata beneath them as shown in Figure 20. We have identified a landslide toe or margin in the northwestern portion of the study area, but are unable to constrain its scale and thickness. The fault bounded graben interpreted from the seismic profiles may have pre-disposed this part of the Traverse Mountains to channel landsliding into the topographic low down-slope (Figure 22).

Suggestions for future study

The purpose of this study is to describe the mapped landslide using an integrated methods approach. Our methods probed various depths of the south slope of the Traverse Mountains in order to describe morphology, geologic units and find evidence of landslide movement. This study and methods could be improved in several areas, providing a more accurate depiction of the geologic development of the study area previously mapped as a landslide.

The original seismic survey was larger in extent than those profiles presented in this study. Seismic surveys were also conducted on areas of the Traverse Mountain to the north-west, and east of the study area (1 and 0.3 km away respectively). These profiles have not yet been processed but may help contribute to the subsurface model of the basal reflector we

interpreted. Processing and correlating the profiles in the surrounding areas may reveal a more accurate trend in dip, topography, and fault trends. Although the method of 2D seismic surveying with a vibroseis source was effective in imaging a horizon 100-200 m below the surface, we were unable to accurately resolve any lithologic boundaries or horizons shallower than 90 m below the ground surface due to the low-frequency nature of the source and possibly due to reduced CDP fold of cover at shallower depths. In order to conclude with more confidence that the volcanic sequence does contain one or more landslides, seismic reflection surveys could be conducted with a higher frequency source so as to image possible glide surfaces within the Oligocene-age volcanic rocks at shallower levels. Higher frequency sources suffer greater attenuation at depth. This present study pursued a conventional two-layer, "refraction static" approach for modeling time shifts due to lateral velocity variations in volcanic materials above the basal reflector. A possibly more accurate approach might be to construct the velocity model using seismic tomography, especially considering the diving wave character of the first arrivals on the shot records.

The drilling project of the south slope of the Traverse Mountains was extensive and covered several square kilometers of the study site and surrounding area. The depth and resolution limitations of the sonic drilling method did not allow for the positive and correlative identification of a landslide glide plane. To effectively calibrate the seismic profiles and identify the horizon imaged, at least two boreholes (possibly cored) to at least a depth of 100-150 m is recommended. Boreholes of this depth may aid in describing the nature of the volcanic body, its geometry, architecture, larger scale alteration patterns and most importantly, the contact with the basal reflector.

A crucial part of landslide mitigation and study involves careful monitoring of water saturation of the rock body in question. Most landslides in Utah are linked with runoff and spring melt water introduced into an already weakened lithology (Biek 2005b). Our study did not include sampling of the wells for water content installed throughout the study area since 2007. Monitoring of the water content in these wells, including fluctuation and identification of any major aquifers may show regions of perched water tables and their proximity to the more heavily hydrothermally altered block and ash units.

Conclusion

The poorly structured and chaotic Tertiary volcanic deposits that mantle much of the Traverse Mountains in the Wasatch Range of northern Utah present an enigma for engineering studies attempting to assess landslide potential. Although geologic maps published by state and federal agencies may show discrete boundaries between landslide (allochthonous) materials and adjacent intact (autochthonous) geologic formations, the landslide designation is often difficult to verify with certainty. Our ability to sample the shallow subsurface with trenches, boreholes, and 2D seismic reflection worked together to describe the larger-scale geomoetry of the volcanic rocks on the southern flank of the Traverse Mountains. Coupled with LiDAR, surface geologic mapping can provide structural details not readily apparent from one method alone. For example, the integration of LiDAR and geologic mapping helped identify a normal fault corresponding to a drainage bordering the western margin of the mapped landslide (Biek, 2005a). LiDAR provided high-resolution surface imagery that revealed subtle contrasting textures of the landslide and surrounding volcanic body, as well as show in greater detail drainages and margins of 'old' landslide morphology.

The seismic reflection method helped to the correlate faults mapped or inferred at the surface to faults at depth. The seismic method also succeeded in imaging a major reflector boundary within or near the base of the Oligocene-age volcanic rocks . As discussed by Tingey et al. (2007) for their study of the Little Valley landslide, a younger deposit located on the northern flank of Traverse Mountains, the basal reflector underlying a putative landslide may either represent a glide surface or the top of a relatively intact volcanic (or other geologic) unit underlying its weathered products. Without the context provided by geologic mapping and borehole logging, it may not be possible to accurately interpret a basal reflector one way or the

other. Near the surface of our study area, within trenches and boreholes, we observe a heterogeneous body of volcanic rock, with a wide range of structural modification and lithologic alteration. The low-frequency vibroseis method allowed us to image the deeper structure of the landslide, but emphasizing more of the homogenous nature of the deposit, irrespective of the finer scale features.

The study site on the south slope of the Traverse Mountains has a surface morphology, internal structure, and composition consistent with a history of landsliding that could have commenced with the original deposition and flow of Oligocene volcanic lavas. Hydrothermal and structural weakening of the volcanic body shows signs of landsliding in the western margin of the study area. The combination of hydrothermal alteration, mechanically weak block and ash flow tuffs, and deformation associated with Basin and Range extension all suggest that the study area may not simply be a single mass of rock that has slid down-slope, but is best characterized as an amalgamation of volcanic debris, possible successive landslides, and normal faulting.

References

Ashland, F.X., 2009, Snowmelt-Induced Ground-Water Fluctuations in Selected Northern Utah Landslides - Preliminary Results from the 2007-08 Landslide water year, Utah Geological survey, Open-File Report 550.

Ashland, F.X., and Christenson, G.E., 2007, Assessing the Stability of Landslides – Overview of Lessons Learned from Historical Landslides in Utah, Proceedings for the 40th Symposium on Engineering Geology and Geotechnical Engineering: Logan, Utah State University, 17 p., compact disk.

Best, M.G., and Christiansen, E.H., 1991, Limited Extension During Peak Tertiary Volcanism, Great Basin of Nevada and Utah: Journal of Geophysical Research, v. 96 no. B8, p. 509-528.

Biek, R.F., 2005a, Geologic map of the Lehi Quadrangle and part of the Timpanogos Cave Quadrangle, Salt Lake and Utah Counties, Utah, Lehi Quadrangle Geologic Map, 02HQAG0055, scale 1:24 000, 2 sheets.

Biek, R.F., 2005b, The Traverse Mountains; New Geologic Maps and Explosive Suburban Growth, Utah Geological Survey, Survey Notes, v. 37 no. 2.

Bláha, P., 2009, Landslide and its complex investigation: Acta Montanistica Slovaca, v. 14, no 3 p. 221-231.

Bogoslovsky, V.A., and Ogilvy, A.A., 1977, Geophysical Methods for the Investigation of Landslides: Geophysics, v. 42 no. 3, p. 562-571.

Bordoni, P., Haines, J., Di Giulio, G., Milana, G., Augliera, P., Cercato, M., Martelli, L., and Cara, F., 2007, Cavola Experiment Site: Geophysical Investigations and Deployment of a Dense Seismic Array on a Landslide: Annals of Geophysics, v. 50 no. 5, p. 627.

Bruhn, R.L., Gibler P.R., and William T.P., 1987, Rupture characteristics of normal faults: an example from the Wasatch fault zone, Utah: Continental Extensional Tectonics: Geological Society Special Publication, v. 28, p. 337-353.

Bruno, F., and Marillier, F., 2000, Test of High-Resolution Seismic Reflection and Other Geophysical Techniques on the Boup Landslide in the Swiss Alps: Surveys in Geophysics, v. 21, p. 333-348.

Census Bureau, U.S., 2009, State & County QuickFacts: Utah and Salt Lake Counties: http://quickfacts.census.gov/qfd/states/49000.html (January 2010).

Charbonnier, S.J., and Gertisser, R., 2008, Field observations and surface characteristics of pristine block-and-ash flow deposits from the 2006 eruption of Merapi Volcano, Java, Indonesia: Journal of Volcanology and Geothermal Research, v. 177, p. 971-982.

Elliott, A.H., and Kirschbaum, M.J., 2007, The Preliminary Landslide History Database of Utah (1850-1978), Volume Open-File Report 514, Utah Geological Survey.

Fisher, R.V., and Grant, H., 1982, Mt. Pelée, martinique: may 8 and 20, 1902, pyroclastic flows and surges: Journal of volcanology and geothermal research v. 13, p. 339-371.

Glade, T., Stark, P., and Dikau, R., 2005, Determination of potential landslide shear plane depth using seismic refraction—a case study in Rheinhessen, Germany: Bulletin of Engineering Geology and the Environment, v. 64, p. 151-158.

Gomez C.; Lavigne, F.H., Hadmoko, D.S., Lespinasse, N., and Wassmer, P., 2009, Block-and-ash flow deposition: A conceptual model from a GPR survey on pyroclastic- flow deposits at Merapi Volcano, Indonesia: Geomorphology, v. 110, p. 118-127.

Griffiths, J.S., 1999, Proving the occurrence and cause of a landslide in a legal context: Bulletin of Engineering Geology, v. 58, p. 75-85.

Jongmans, D., and Garambois, S., 2007, Geophysical investigation of landslides: a review: Bulletin de la Societe Geologique de France, v. 178, no 2, p. 101-112.

Kalderon-Asael, B., Katz, O., Aharonov, E., and Shmuel, S., 2008, Modeling the relation between area and volume of landslides Ministry of National Infrastructures Geological Survey of Israel, Jerusalem, Steering Committee for Preparation for Earthquakes, Report GSI/06/2008.

Mario, P., 2003, Observation of Surface Features on an Active Landslide, and Implications for Understanding its History of Movement: Natural Hazards and Earth System Sciences, v. 3, p. 569-580.

McBride, J.H., Stephenson, W. J., Thompson, T.J., Harper, M.P., Eipert, A.A., Hoopes, J.C., Tingey, D.G., Keach, II, R.W., Okojie-Ayoro, A.O., Gunderson, K.L., Hicks, T.C., Spencer, C.J., Meirovitz, C.D., Worley, D.M., and Yaede, J.R., 2008, A Geophysical Investigation of Shallow Deformation Along an Anomalous Section of the Wasatch Fault Zone, Utah, USA: Environmental & Engineering Geoscience, v. 14 no 3, p. 183-197.

McBride, J.H., Stephenson, W.J., Williams, R.A., Odum, J.K., Worley, D.M., Keach II, R.W., South, J.V., Brinkerhoff, R.A., and Okojie-Ayoro, A.O., 2010, Shallow subsurface structure of the Wasatch Fault, Provo Segment, Utah, from an integrated compressional- and shear-wave seismic reflection profile with implications for fault structure and development: Geological Society of America Bulletin, v. 122 no. 11/12, p. 1731-1745.

McCann, D.M., and Foster, A., 1990, Reconnaissance geophysical methods in landslide investigations: Engineering Geology, v. 29, p. 59-78.

Miller, E.L., and Gins, P.B., 1989, Cretaceous crustal structure and metamorphism in the hinterland of the Sevier thrust belt, Western U.S. Cordillera: Geology, v. 17, p. 59-62.

Moon, V., and Simpson, C.J., 2002, Large-scale mass wasting in ancient volcanic materials: Engineering Geology, v. 64, p. 41-64.

Murphy, P.J., and Gwynn, J.W., 1979, Geothermal Investigations at Crystal Hot Springs, Salt Lake County Utah, Report of Investigation, Utah Geological and Mineral Survey, Report no. 139, Contract DE-AS07-77ET28393.

Stephenson, W.S., Williams, R.A., Odum, J.K., McBride, J.H., and Tomlinson, I., 2011, Characterization of intrabasin faulting and deformation for earthquake hazards in southern Utah Valley, Utah, from high-resolution seismic imaging: Bulletin of the Seismological Society of America., in review.

Tingey, B.E., McBride, J.H., Thompson, T.J., Stephenson, W.J., South, J.V., and Bushman, M., 2007, Study of a prehistoric landslide using seismic reflection methods integrated with geological data in the Wasatch Mountains, Utah, USA: Engineering Geology, v. 95, p. 1-29.

Tooker, E.W., and Roberts, R.J., 1970, Upper Paleozoic Rocks in The Oquirrh Mountains and Bingham Mining District, Utah: United States Government Printing Office, Geological Survey Professional Paper 629-A.

University of Utah, 1984, Flooding and Landslides in Utah - an Economic impact analysis: University of Utah Bureau of Economic and Business Research, Department of Community and Economic Development and Utah Office of Planning and Budget, p. 123.

Van Den Eeckhaut, M., Poesen, J., Verstraeten, G., Vanacker, V., Nyssen, J., Moeyersons, J., Van Beek, L.P.H., and Vandekerkhove, L., 2006, Use of LIDAR-derived images for mapping old landslides under forest: Earth Surface Processes and Landforms, v. 32, p. 754-769.

Van Den Eeckhaut, M., Verstaeten, G., and Poesen, J., 2007, Morphology and internal structure of a dormant landslide in a hilly area: The Collinabos landslide (Belgium): Geomorphology, v. 89, p. 258-273.

Visitor Center, Salt Lake city Utah, 2010, Demographics, www.saltlakecityutah.org, (January 2011).

Williams, R.A., Pratt, T.L., 1996, Detection of the Base of Slumgullion Landslide Colorado, by Seismic Reflection and Refraction Methods: The Slumgullion Earth Flow: A Large-Scale Natural Laboratory, U.S. Geological Survey Bulletin 2130, Chapter 13, p. 83-89.

Zhang, Z.Y., Chen, S.M., and Tao, L.J., 2002, 1983 Sale Mountain landslide, Gansu Province, China: Reviews in Engineering Geology - Catastrophic landslides: effects, occurrence, and mechanisms - The Geological Society of America, Reviews in Engineering Geology v. 15, p. 149-163.

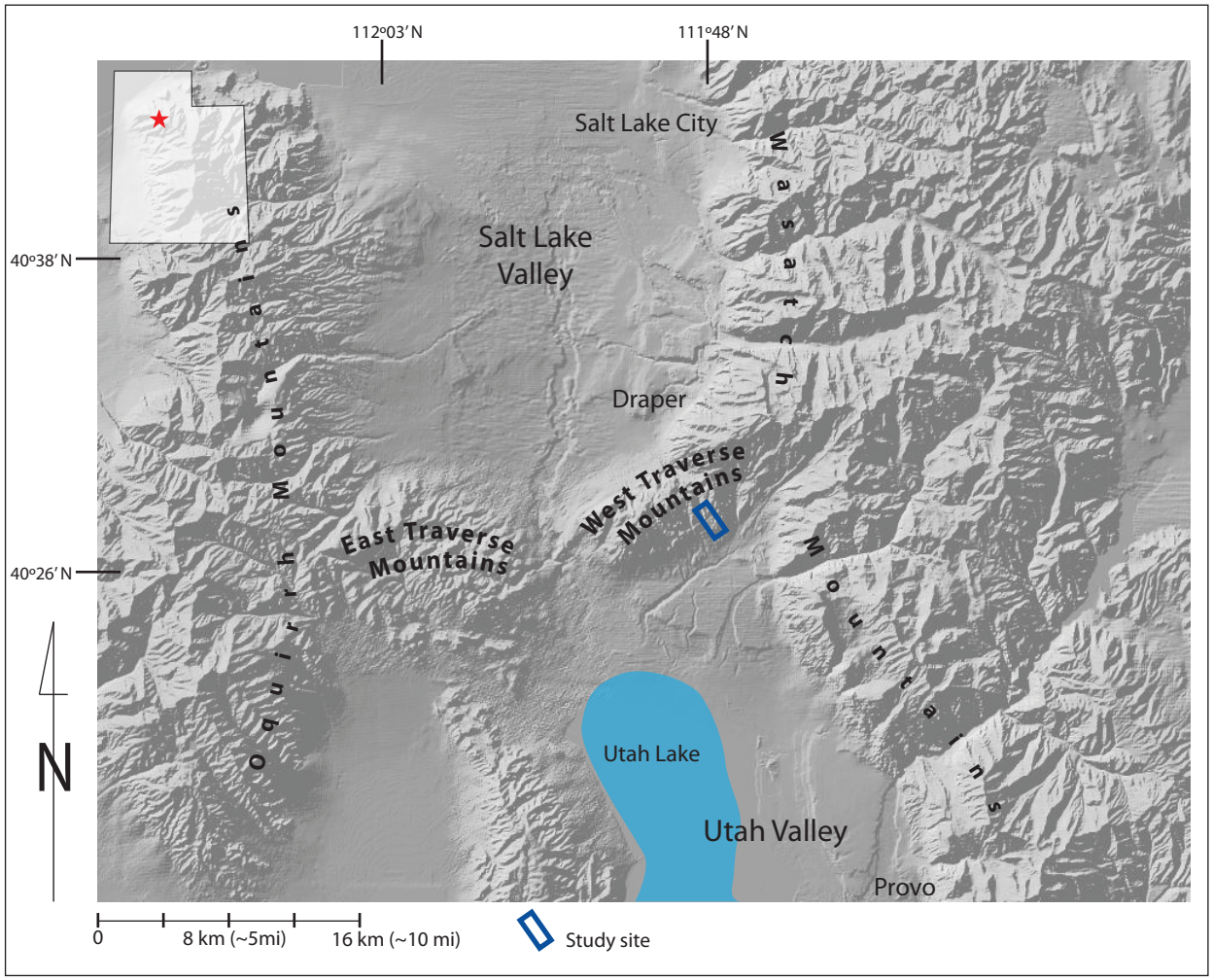

Figure 1 – *The Traverse Mountains are situated between the Salt Lake and Utah valleys. The study area, on the south flank of the West Traverse Mountains (shown in blue rectangle), is a salient of the Wasatch Mountains. (Shaded map relief by Utah GIS portal - http://agrc.its.state.ut.us/)*

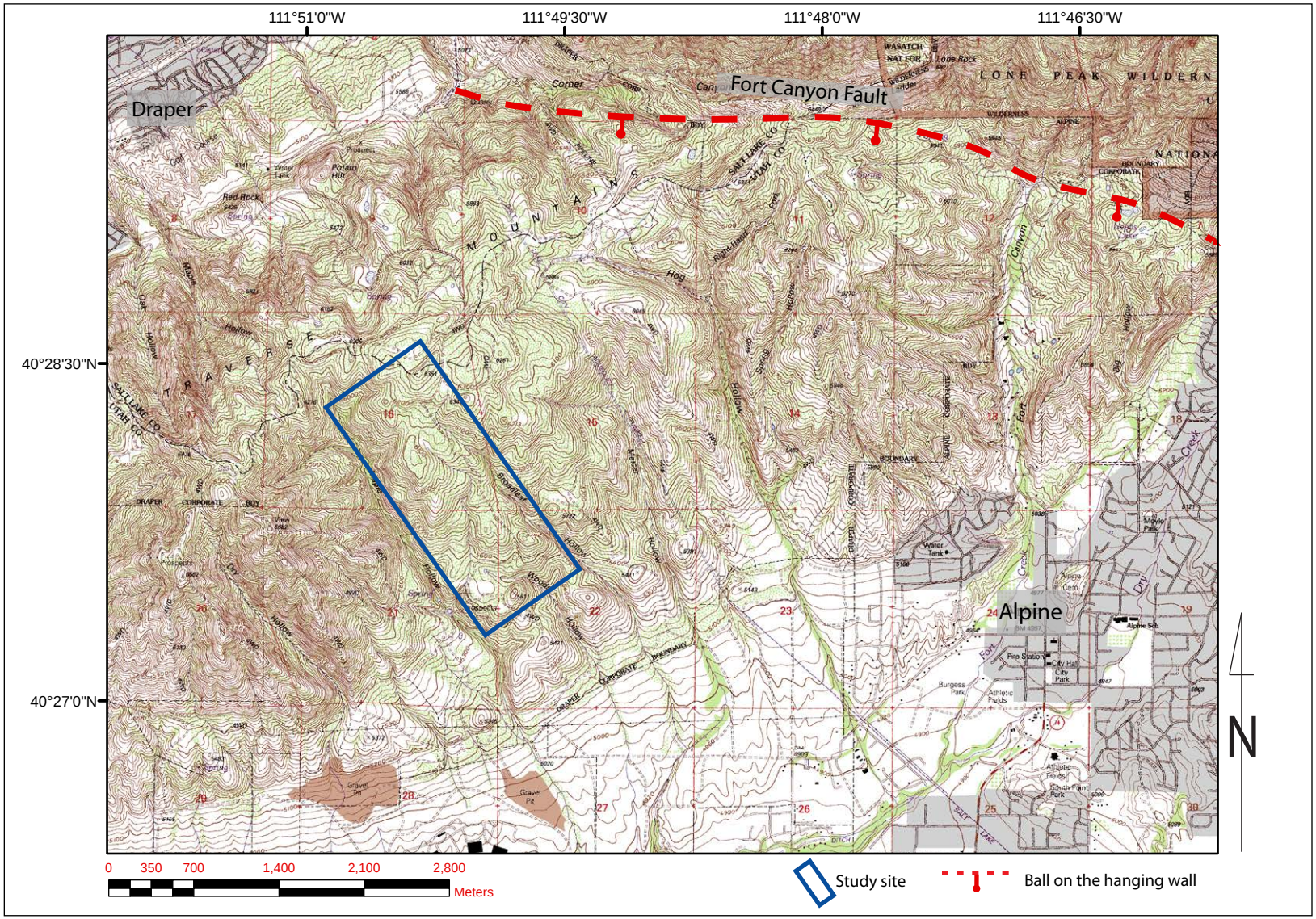

Figure 2 - *A topographic map of a part of the Traverse Mountains. The dashed line represents the Fort Canyon Fault zone, which joins the Salt Lake and Provo segments of the Wasatch Fault system. Our study area is boxed in red, on the southern slope of the Traverse Mountains just below a housing development to the north at the crest. (Topographic map by the USGS, Lehi Quadrangle, 1:24,000 – http://gis.utah.gov)*

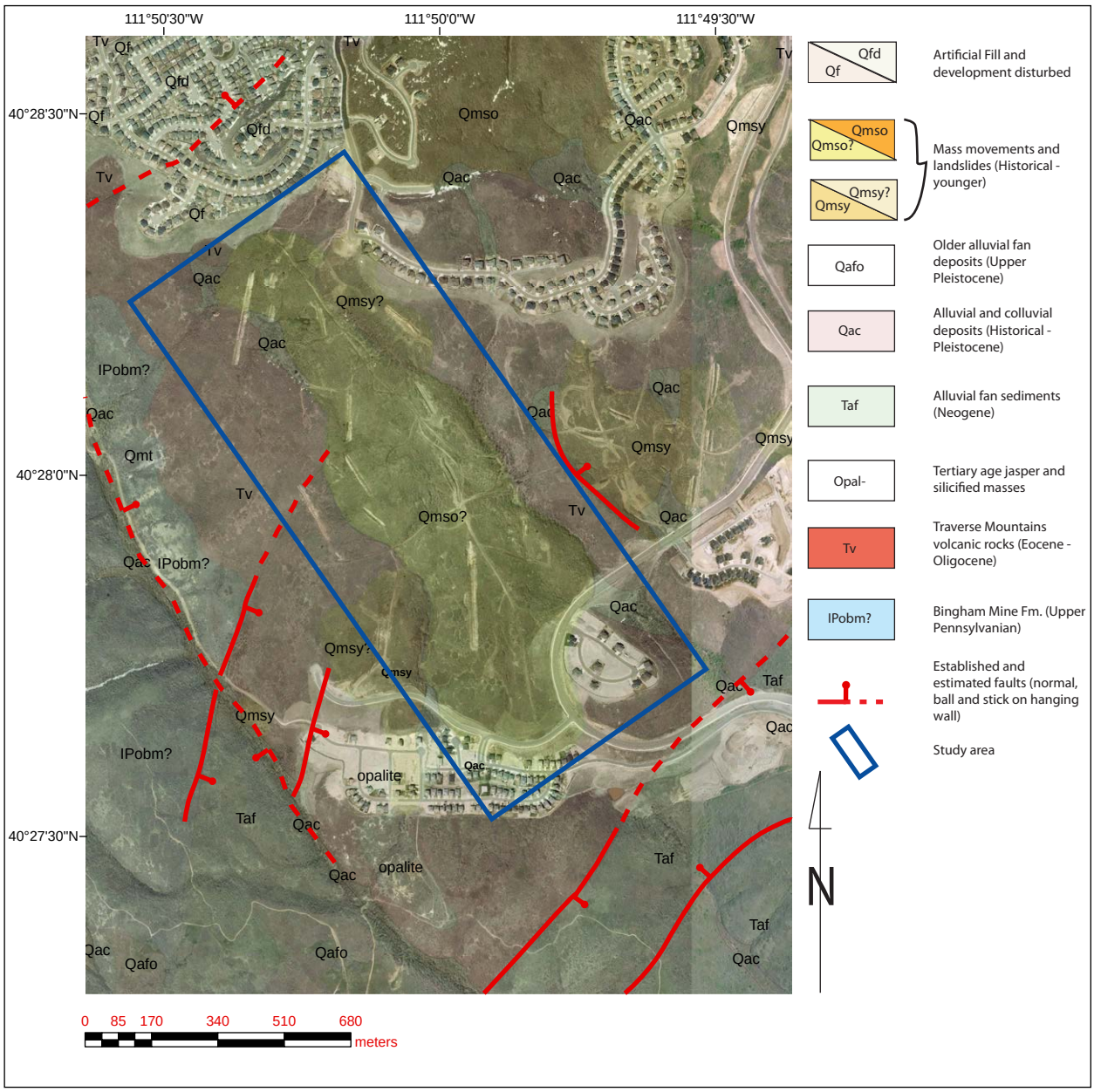

Figure 3 – *Aerial view of the study area (outlined in blue) with faults (red with stick and ball on down thrown side) and geology taken from the Lehi Quadrangle Geologic map (Biek 2005a). Mapped faults are solid red lines and dashed are inferred fault locations. The main housing development is at the crest of Traverse Mountain (north) while some smaller developments are at the base. (Imagery from Utah's GIS portal - Http://gis.utah.gov, 2009 HRO 1 foot color orthophotography - Rick Kelson. Units, ages and descriptions from Biek 2005a)*

Figure 4 - *Photo taken facing north-east on the south slope of the Traverse Mountains. In the far background are the Wasatch Mountains' western front. Houses in the image are approximately 0.8 km (0.5 mi) away on the crest of the landfill material brought in for housing development. Trench 14 is visible in this photo with the light grey exposed rocks and soil excavated in 2007. In the foreground below the houses, is our study area with heavy vegetation. (Photo by John Hoopes, 2010)*

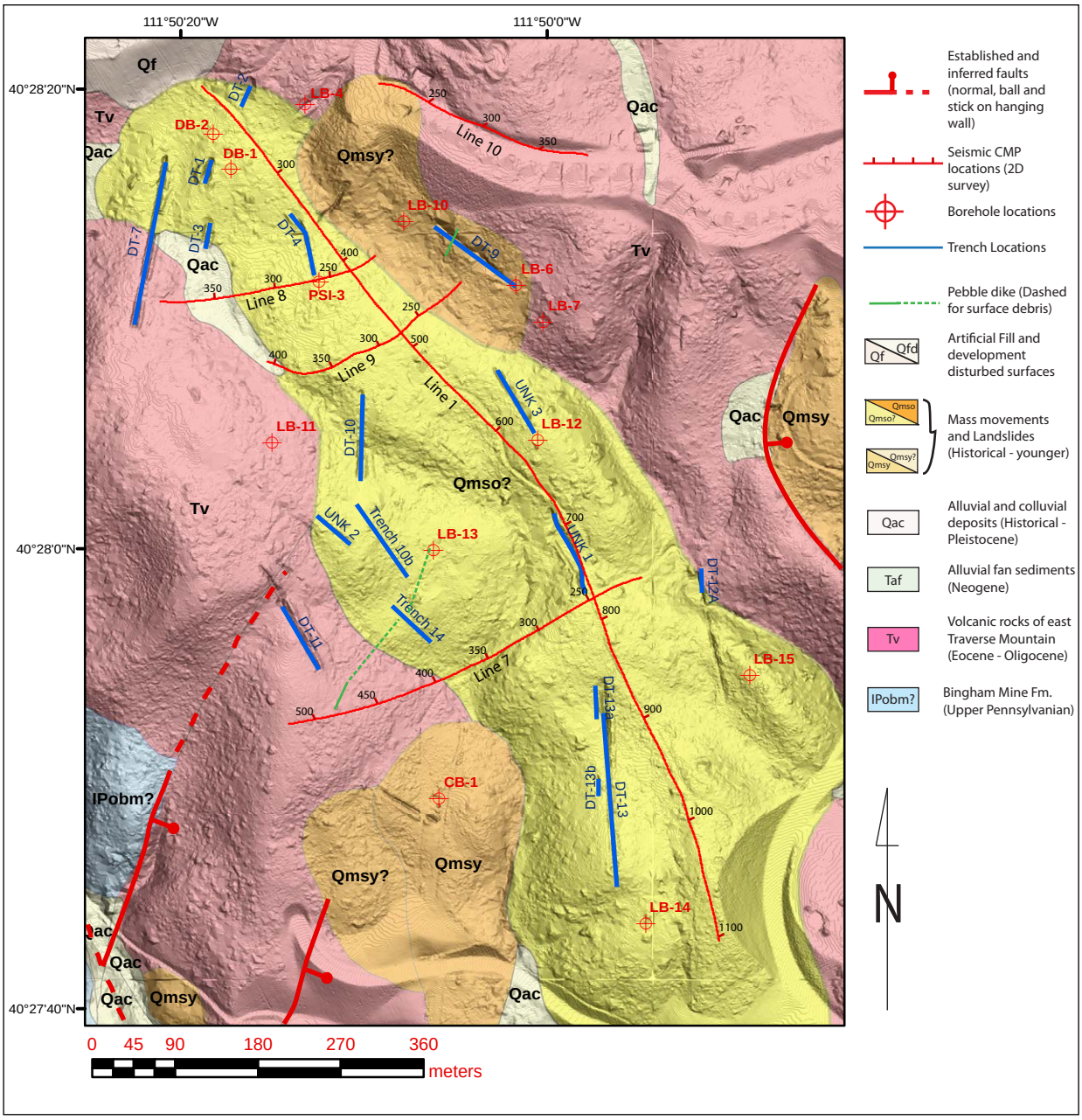

Figure 5a – *Shaded relief map constructed with second return LiDAR data of the study area overlain with Biek's (2005a) geologic map, trenches, boreholes, seismic profiles (CMP locations), and other geologic structure of the south slope. Flat areas are the result of homes and roads.*

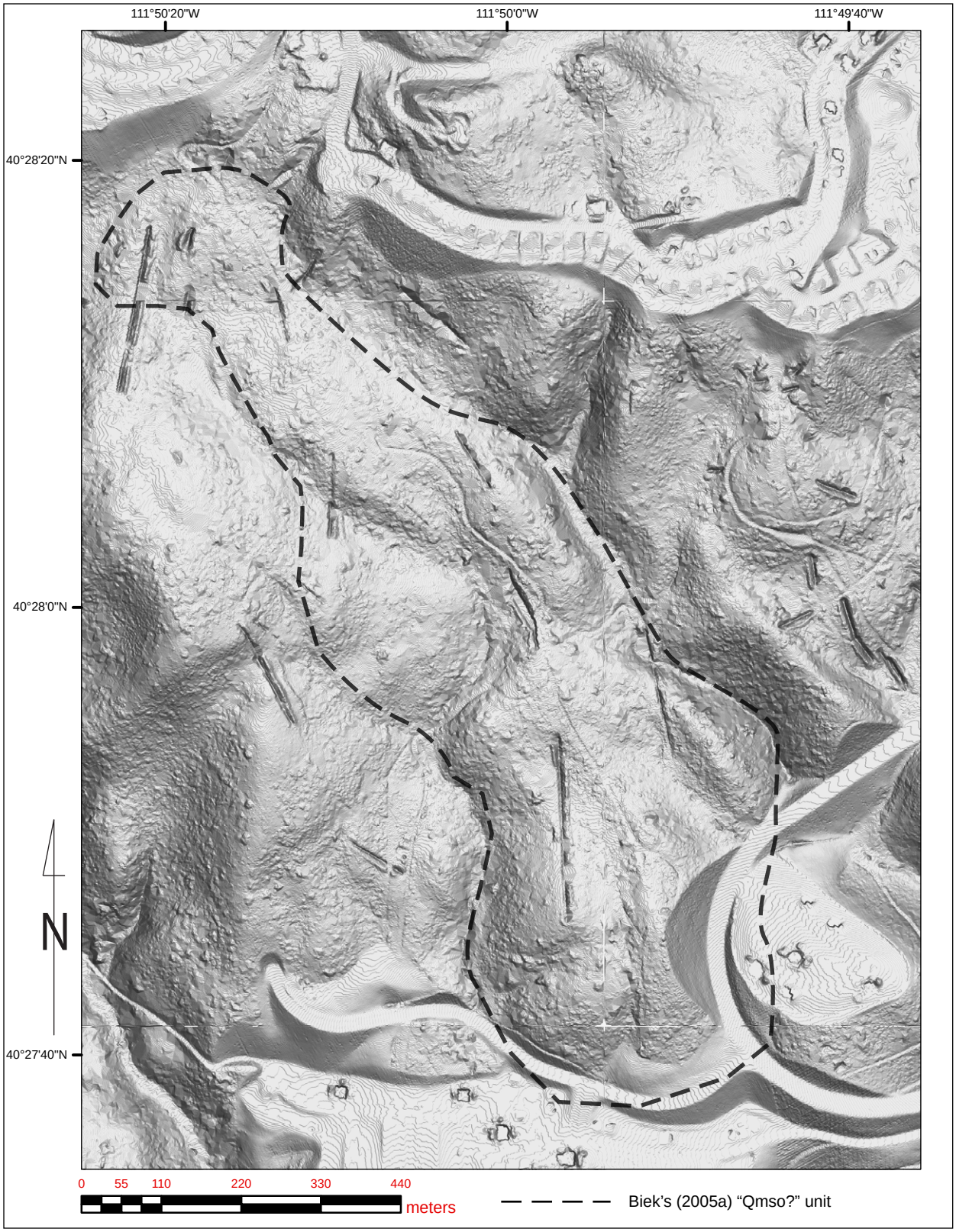

Figure 5b–A *shaded relief map constructed with second return LiDAR data of the study area overlain. Resolution is estimated to be approximately 0.5 meters.*

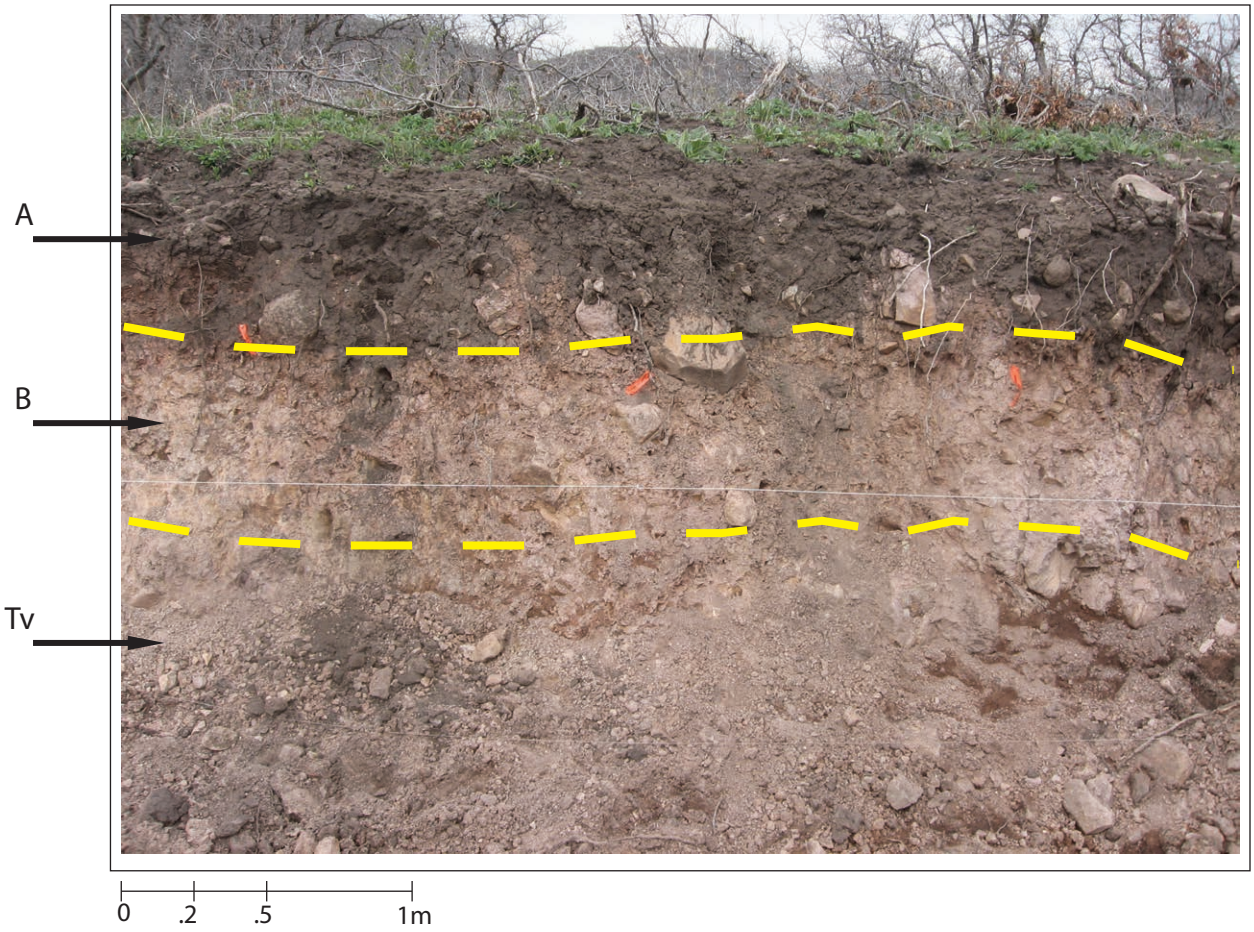

Figure 6 - *The west wall of trench DT-7 (Figure 5a) at 160' from the south end, showing the A and B soil horizons observed in most other trenches. The A horizon is commonly a dark, organic rich soil with some volcanic rock fragments. The B horizon has less organic material with more volcanic rock fragments of various sizes overlying the Oligocene (Tv) volcanic rocks. Thicknesses vary but are approximately 0.5-1 m thick for either soil horizon. (Photo by Geostrata LLC 2007)*

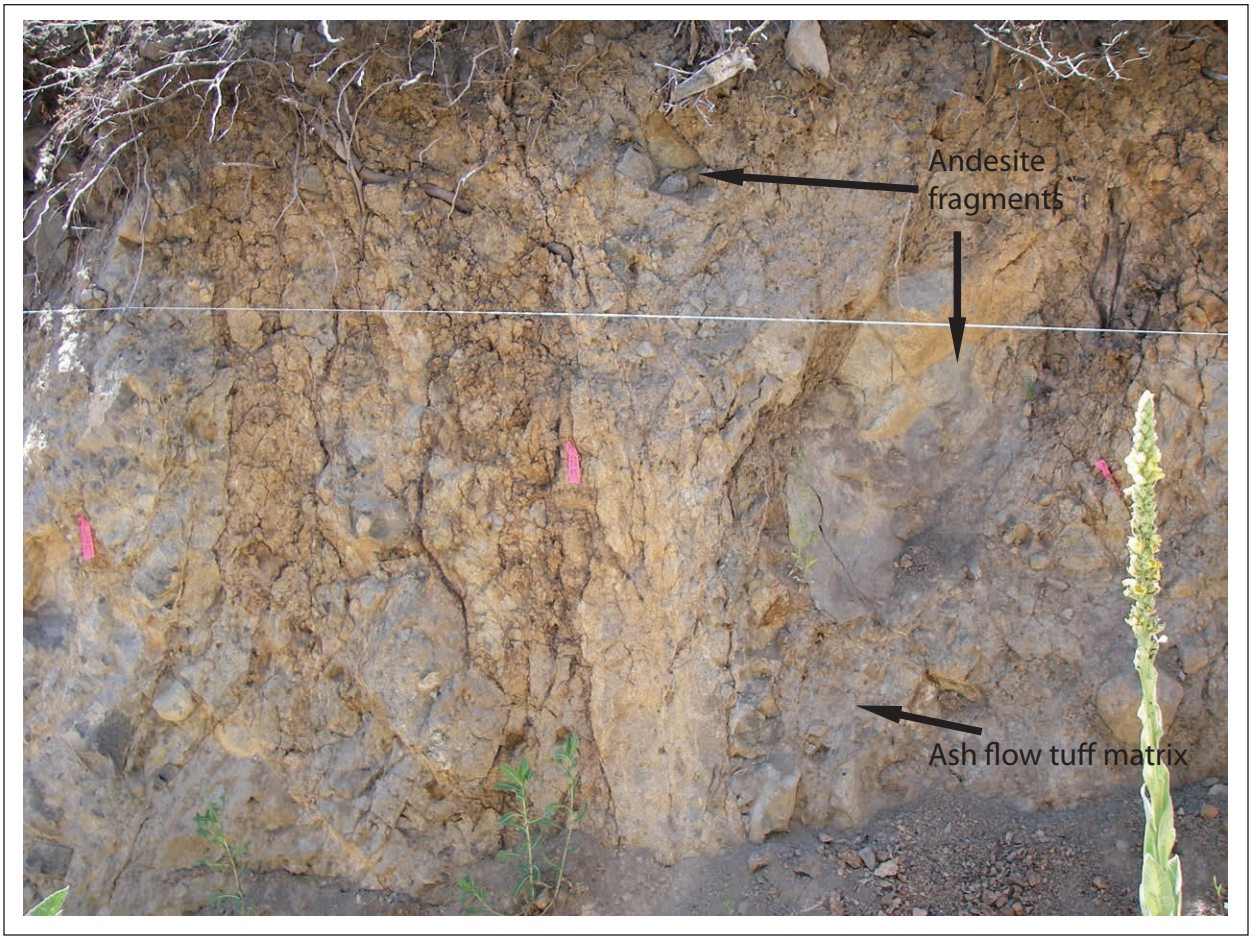

Figure 7 – *A photo of the western wall of trench DT-4 (Figure 5a - at 80 ft /24 m, from the south end) showing an andesite fragment rich block and ash flow tuff. Fragments in the ash flow tuffs range in size from pebbles to boulder size. (Photo by Geostrata LLC, 2007)*

Figure 8 – *A photo of the south-east wall of trench DT-1 (Figure 5a) between 0-20 ft (0-6 m) from the north end. This portion of the trench is dominated by heavily fractured andesite lava. Other, less fractured portions exist throughout the study area. (Photo by Geostrata LLC, 2007)*

Figure 9 - *Photo facing east on seismic line 9. The vibroseis vehicle (IVI Minivibe) with approximately 6 ft (~2.3 m) offset from the geophones. (Photo by Bill Keach, 2007)*

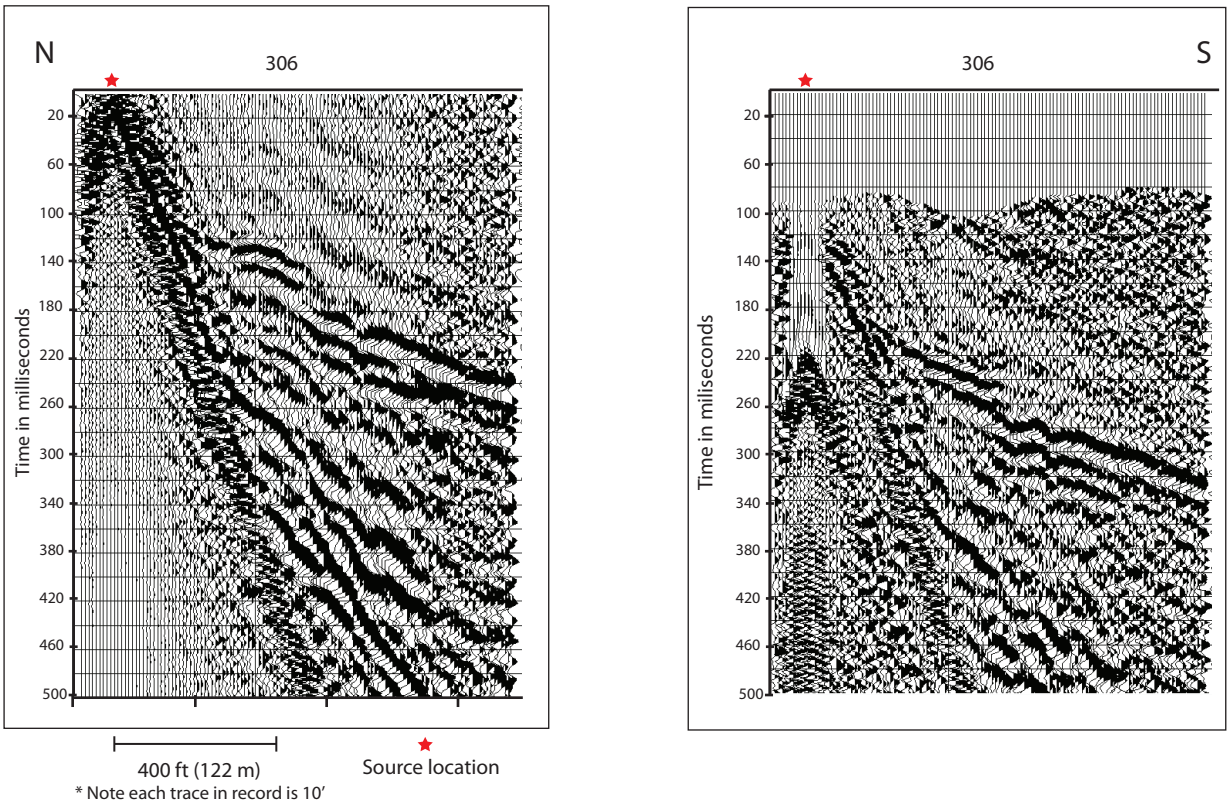

Figure 10 - *Shot record from line 1 (near north end of profile, shooting/advancing southward). Right, shot record (306) showing elevation statics only. Left, the same shot record with filtering (deconvolution, frequency bandpass filtering, and automatic gain control) and refraction static shifts applied. Note strong headwave in this record (left) at approximately 120 ms and offset location 65 (approximately 30 m from north end of profile).*

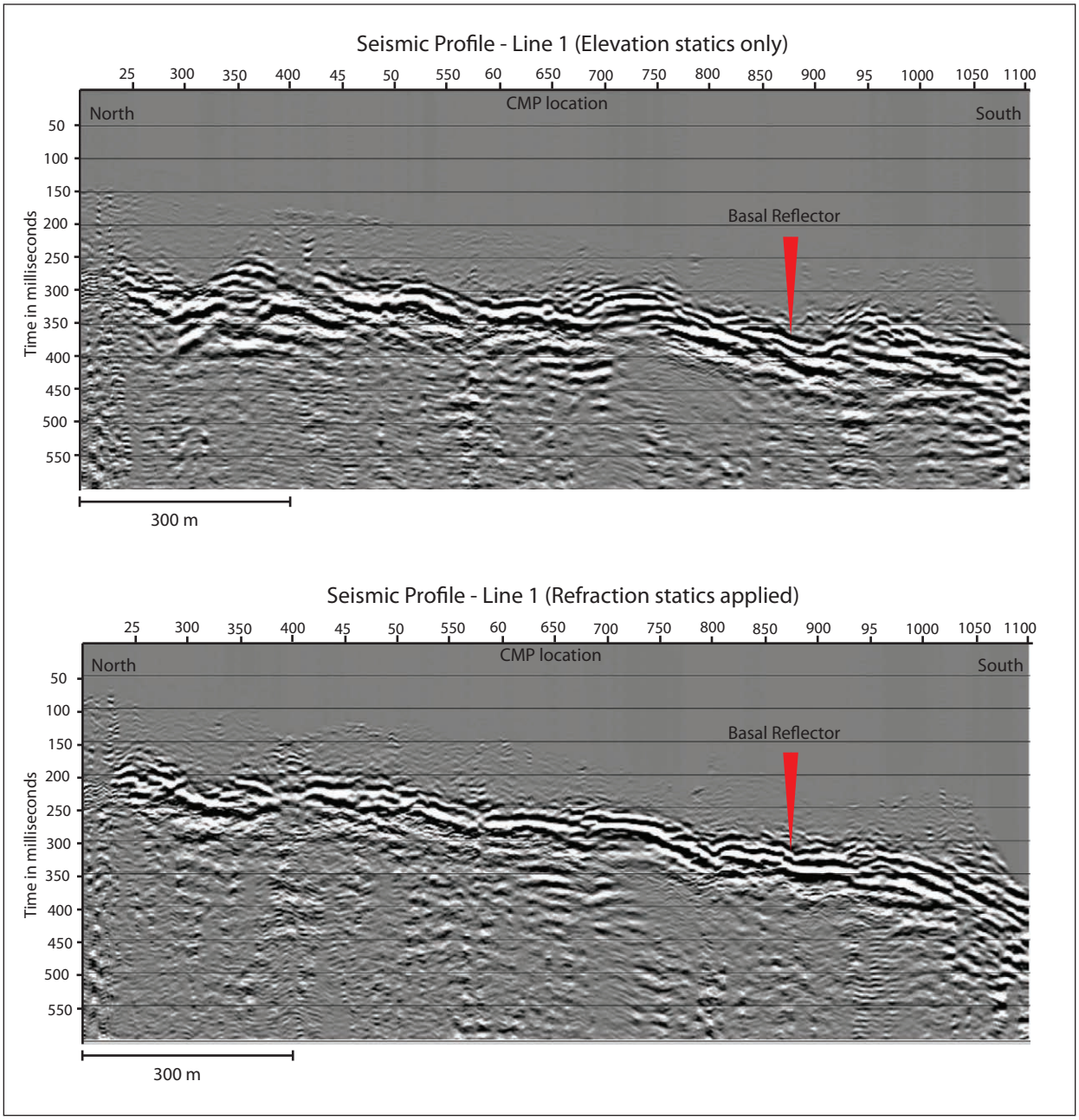

Figure 11 - *Processed profiles of line 1. Top: Seismic processed with elevation statics only applied. Bottom, line 1 processed with refraction statics applied. Note the increase of smoothing and coherency of basal reflector with refraction statics applied.*

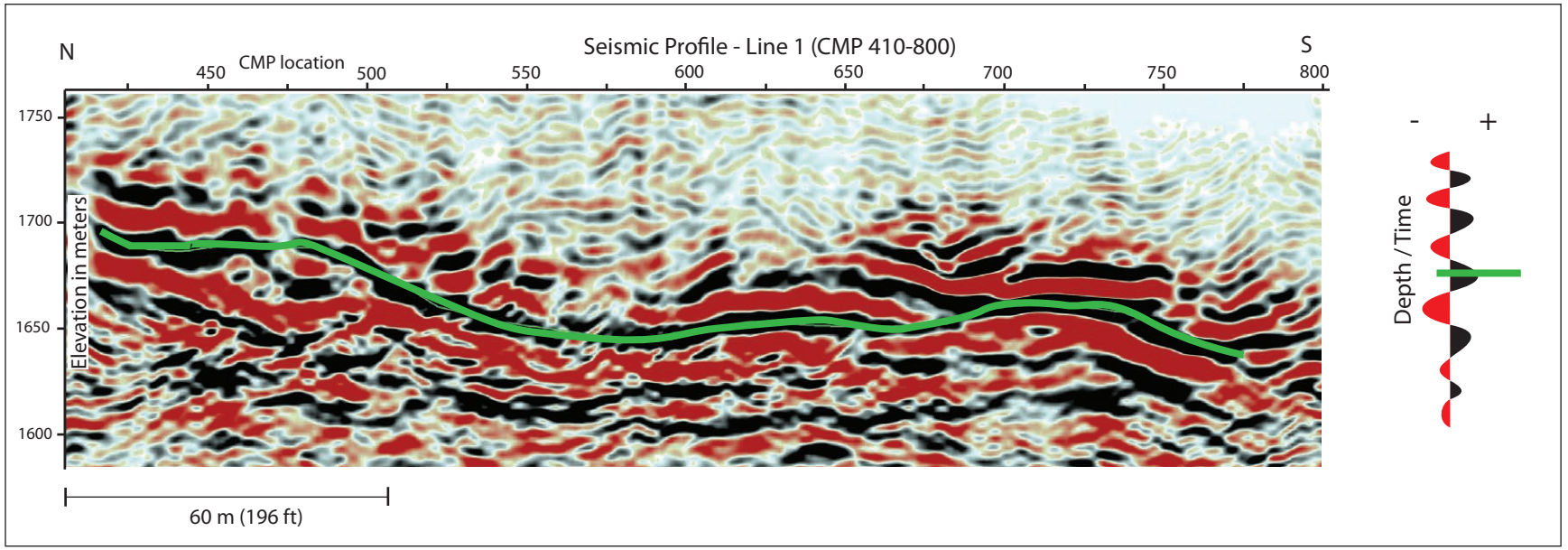

Figure 12- *A portion of line 1 (CMP 410-800) showing the data in greater detail and the interpretation strategy. Our interpretation or 'pick' of the basal reflector was made on the first, most laterally continuous positive amplitude excursion. The wavelet (right) shows the positive excursion in black and green line where the pick would be made. The other major positive excursions or horizons seen in the processed profile were not as laterally continuous and were thus not as suitable for interpretation. This strategy was repeated for lines 7, 8, 9, and 10.*

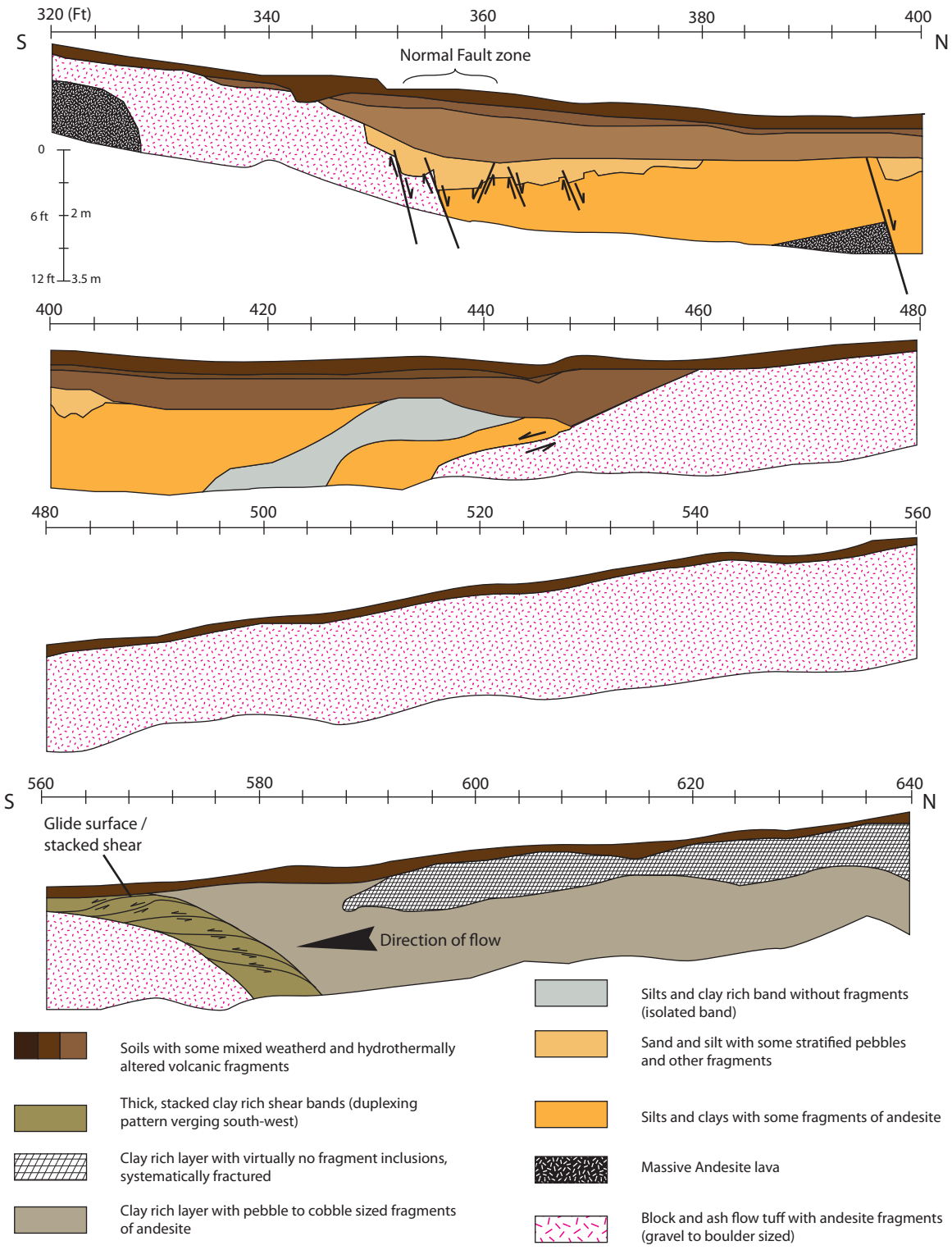

Figure 13 - *Sketch of the west wall of trench DT-7 (Figure 5a) between the 320 and 640 ft (97-195 m) markers (from south end) as sketched by geotechnical geologists in 2007. The original sketches have been digitized for clarity. This portion of the trench crosses a normal fault (350 ft), and a shear plane (568 ft) of a likely landslide flowing south over the volcanic rock units. (Log by Geostrata LLC, 2007 – scale is 1:1, tick-marks represent 4 ft / ~1.2 m segments.)*

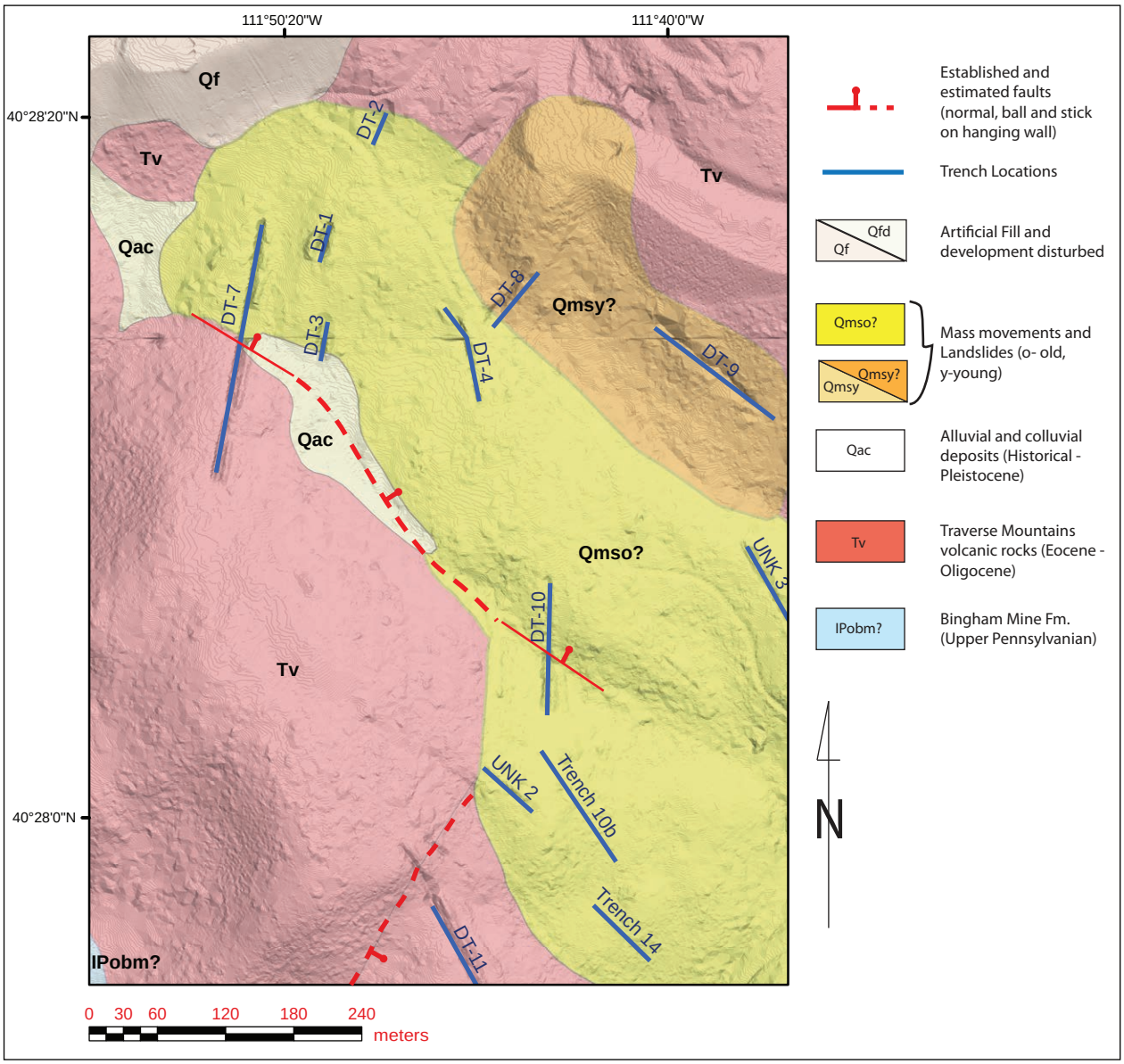

Figure 14 - *The north western portion of the study area with Biek's (2005a) geologic units superimposed on the LiDAR hillshade. Trenches DT-7 and DT-10 both contain a normal fault, striking north-west with the hanging wall to the north-east. The dashed portion between the two segments identified in the trenches is an inference of where the fault may be located and link the two scarps. This fault does not manifest itself at the surface well enough to identify elsewhere.*

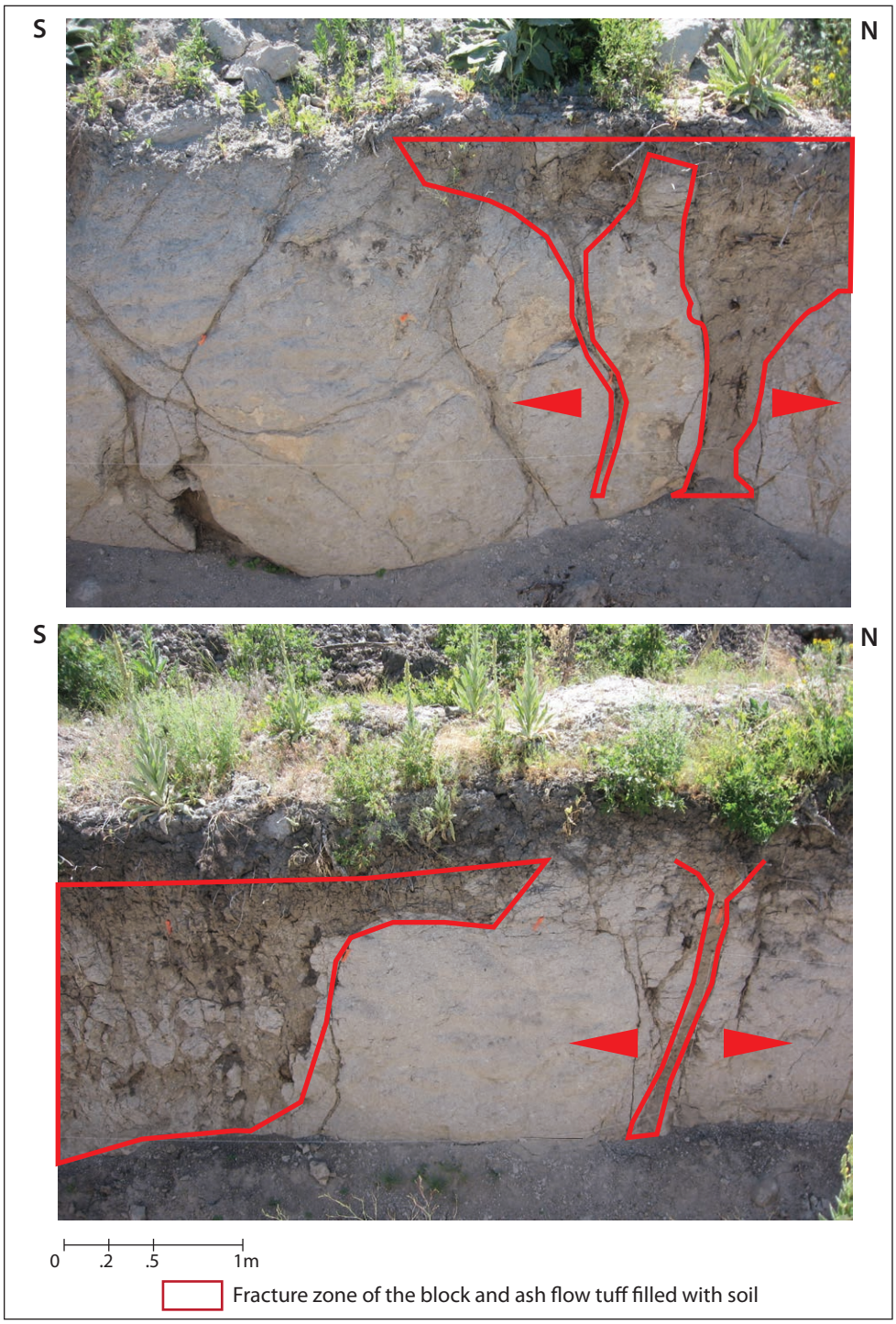

Figure 15 – *Photo of the west wall (top) of Trench UNK-1, 60 ft from the south end (18 m). Transverse fractures filled with B horizon soil. These fractures open in an east-west orientation. West wall photo (bottom) of trench UNK-1 at 132 ft from the south end (40 m), where many fractures were located and are filled with soils, separating portions of the block and ash flow tuff. These fractures are likely the result of extensional activity (landsliding or faulting) since the Palgeogene. Arrows indicate interpreted direction of extension in the block and ash*

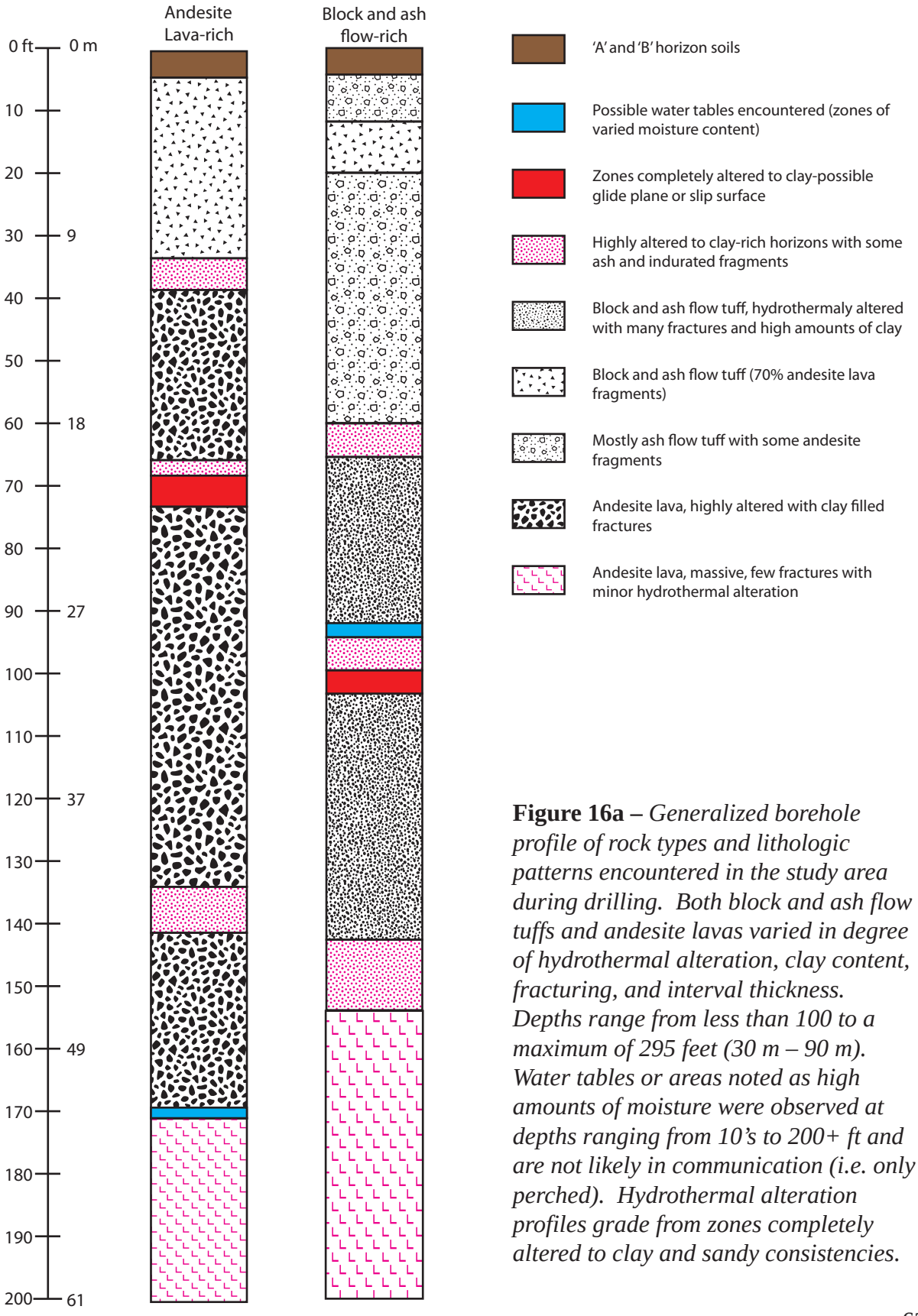

Figure 16a – *Generalized borehole profile of rock types and lithologic patterns encountered in the study area during drilling. Both block and ash flow tuffs and andesite lavas varied in degree of hydrothermal alteration, clay content, fracturing, and interval thickness. Depths range from less than 100 to a maximum of 295 feet (30 m – 90 m). Water tables or areas noted as high amounts of moisture were observed at depths ranging from 10's to 200+ ft and are not likely in communication (i.e. only perched). Hydrothermal alteration profiles grade from zones completely altered to clay and sandy consistencies.*

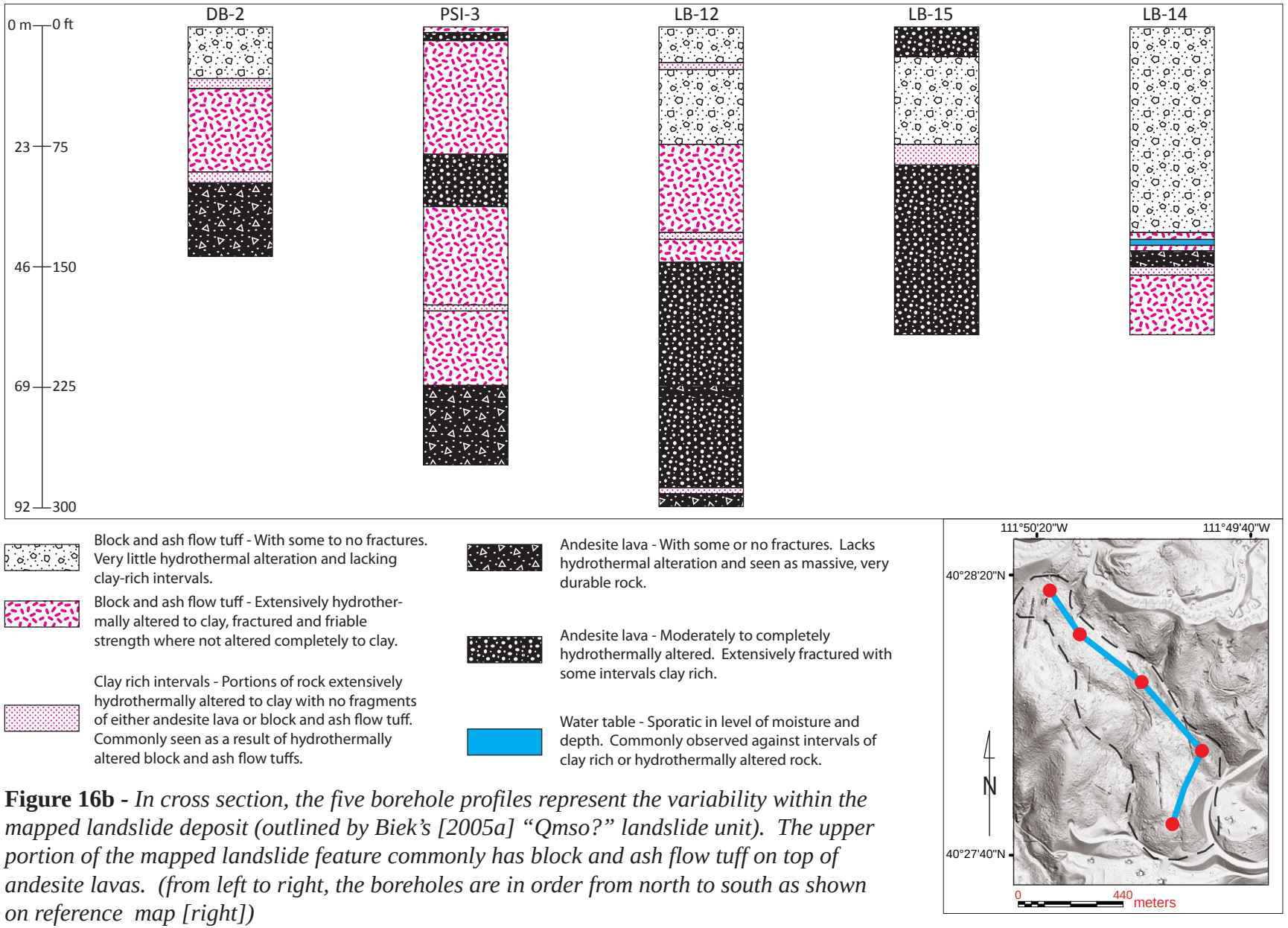

Figure 16b - *In cross section, the five borehole profiles represent the variability within the mapped landslide deposit (outlined by Biek's [2005a] "Qmso?" landslide unit). The upper portion of the mapped landslide feature commonly has block and ash flow tuff on top of andesite lavas. (from left to right, the boreholes are in order from north to south as shown on reference map [right])*

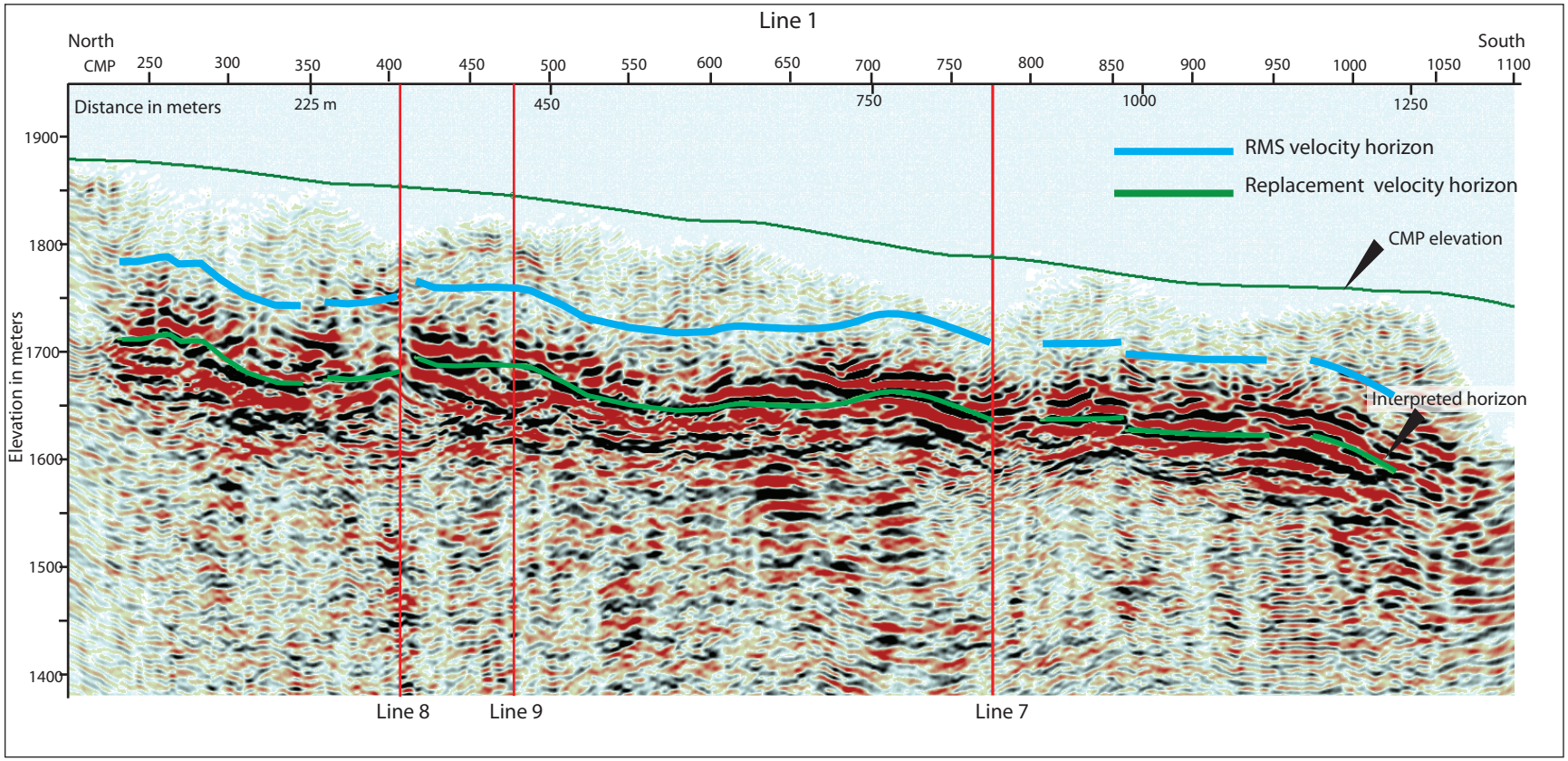

Figure 17 - *Final CMP stacked sections of seismic lines 1, 7, 8, 9, 10. CMP elevations are indicated by green line above. The green line within the seismic profile indicates our interpretation of the main reflector horizon using the replacement velocity for time-depth conversion. The blue line represents where the horizon would be using the RMS velocity model (about 70 m above the replacement velocity model). Elevations on left axis are referenced to the elevation datum of 2000 m, approximately 110 m higher than the greatest elevation in the study area. (Refer to Figure 5a for locations of the seismic profiles)*

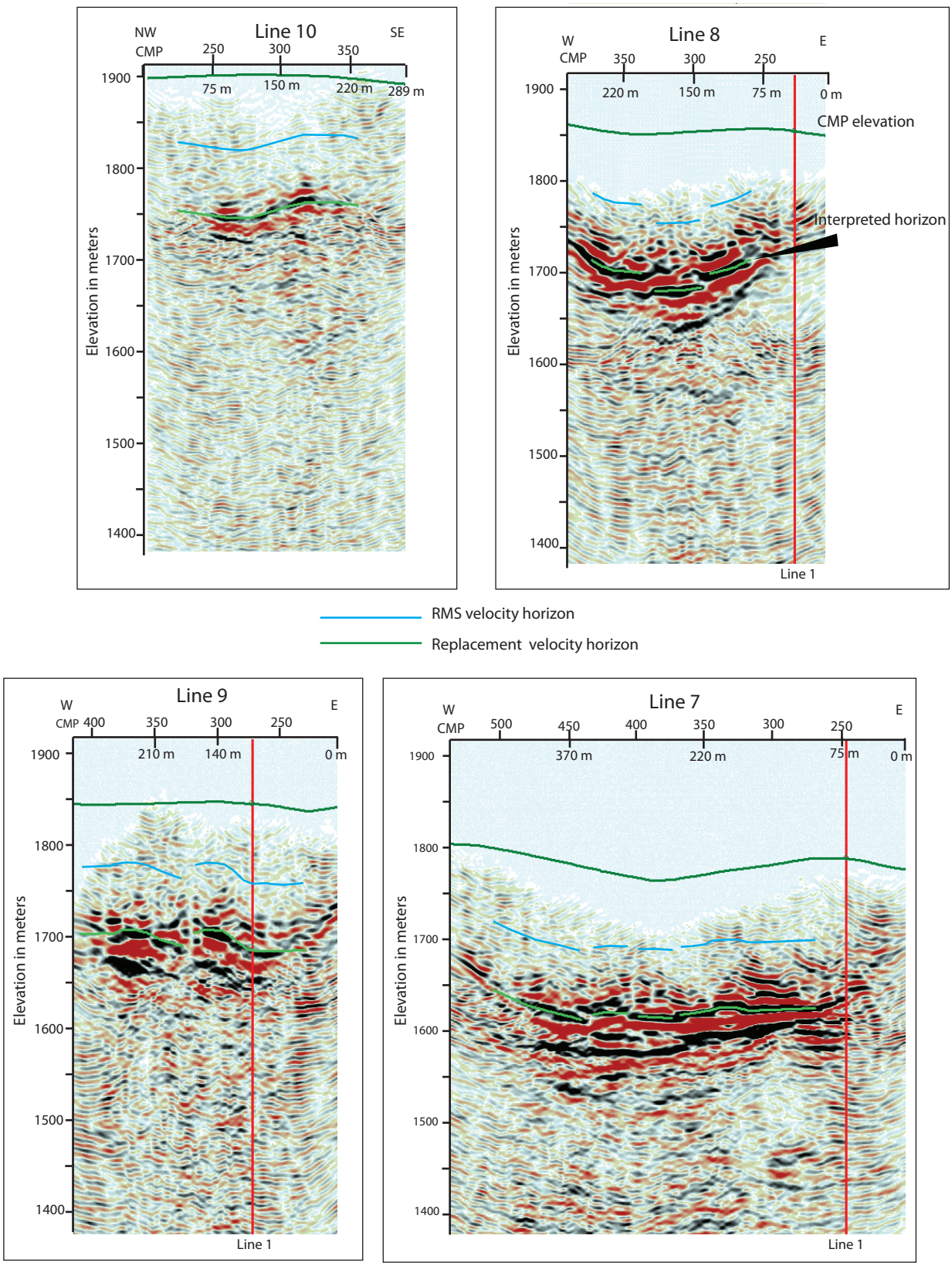

Figure 17 (continued)

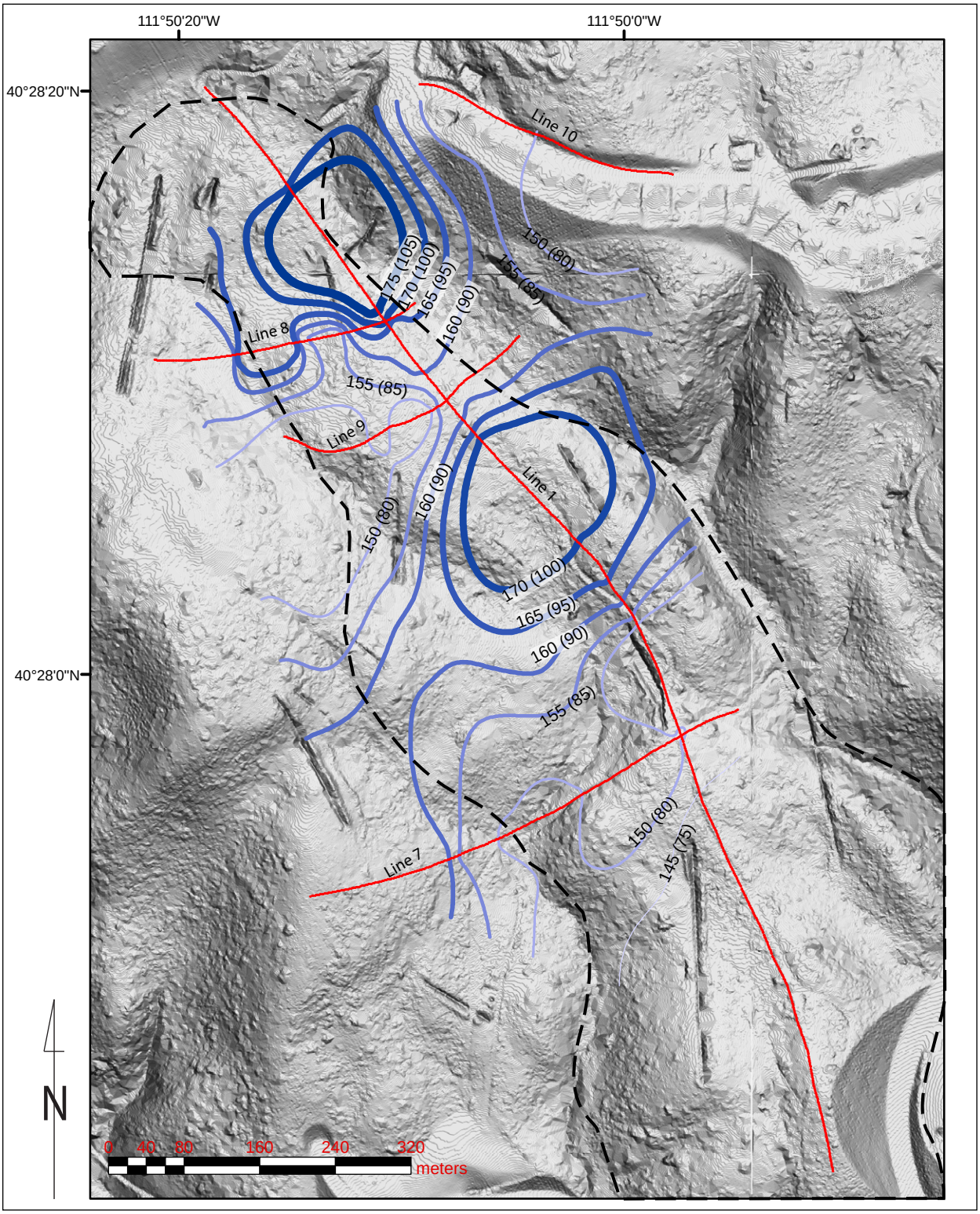

Figure 18 - *Isochore map of the interval between the CMP elevation and the top of the primary reflector. The difference between CDP elevation and the horizon surface gives an approximate thickness of the interpreted Oligocene-age volcanic body. Two distinct thickened portions exist below seismic line 1 separated by a 'saddle' or thin portion beneath line 9. Biek's (2005a) possible mapped landslide unit in dashed line. Using replacement velocities for time-depth conversion offers a conservative thickness estimate while using the RMS velocity provides a reduced estimate of thickness.*

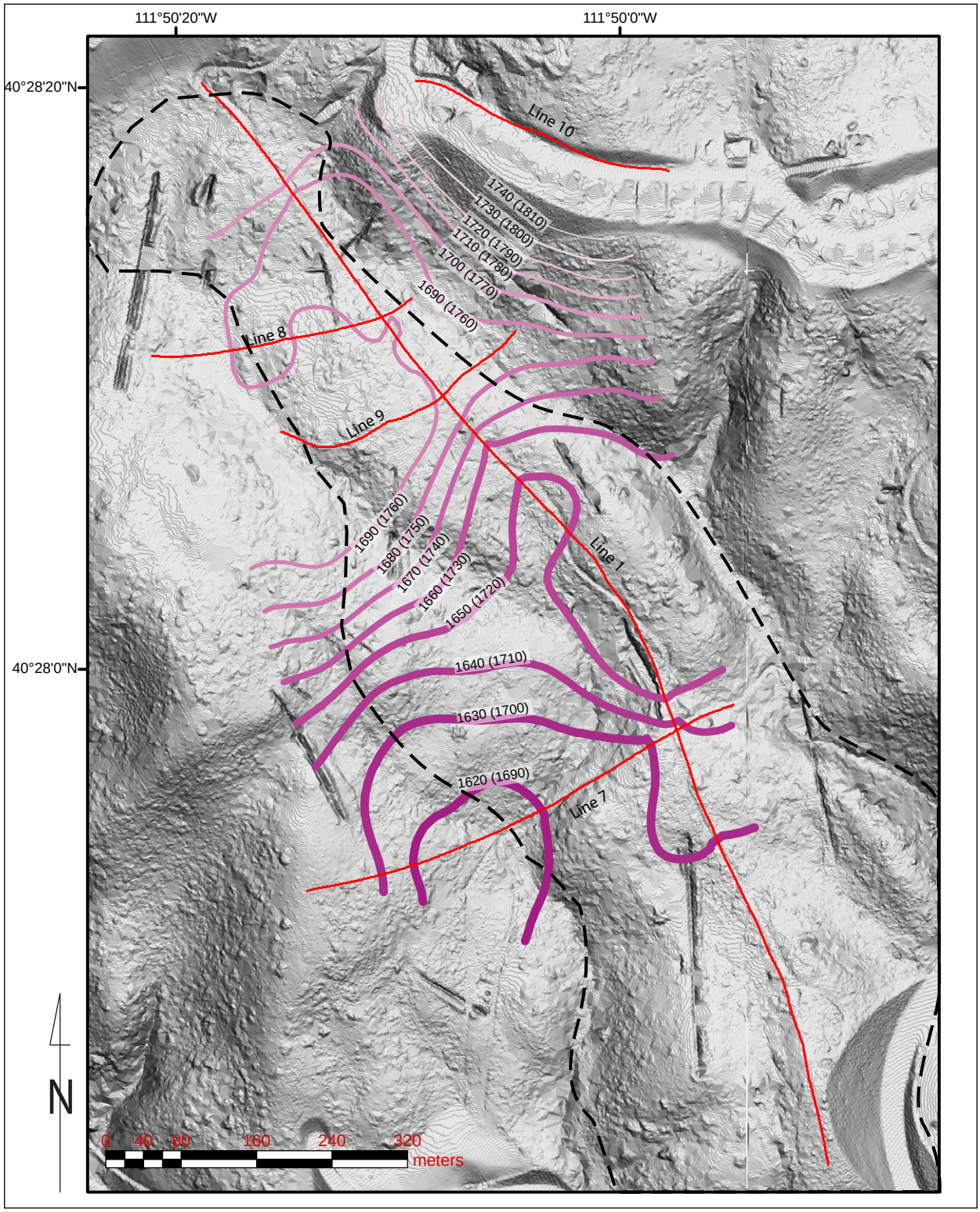

Figure 19 - *Seismic horizon topography as elevation with respect to a datum of 2000 m. Elevations are given from replacement and RMS velocity horizons, (ie. using two different velocities for time-depth conversion) (RMS elevation in parentheses). The general trend of the surface slopes downward, approximately parallel to the surface topography. Note the graben-like depression near the central portion of Line 1 where it crosses lines 8 and 9. Biek's (2005a) possible mapped landslide unit in dashed line.*

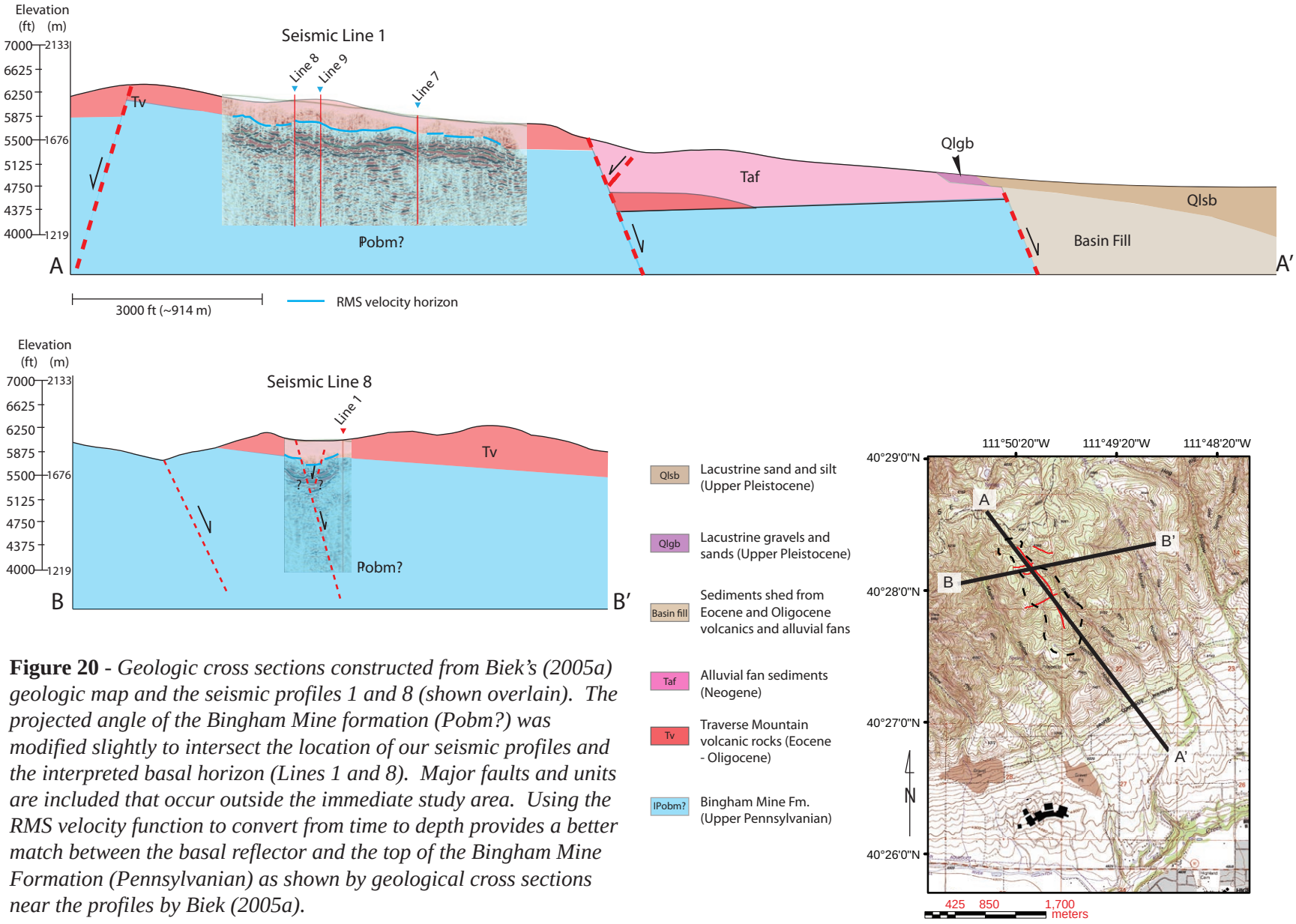

Figure 20 - *Geologic cross sections constructed from Biek's (2005a) geologic map and the seismic profiles 1 and 8 (shown overlain). The projected angle of the Bingham Mine formation (Pobm?) was modified slightly to intersect the location of our seismic profiles and the interpreted basal horizon (Lines 1 and 8). Major faults and units are included that occur outside the immediate study area. Using the RMS velocity function to convert from time to depth provides a better match between the basal reflector and the top of the Bingham Mine Formation (Pennsylvanian) as shown by geological cross sections near the profiles by Biek (2005a).*

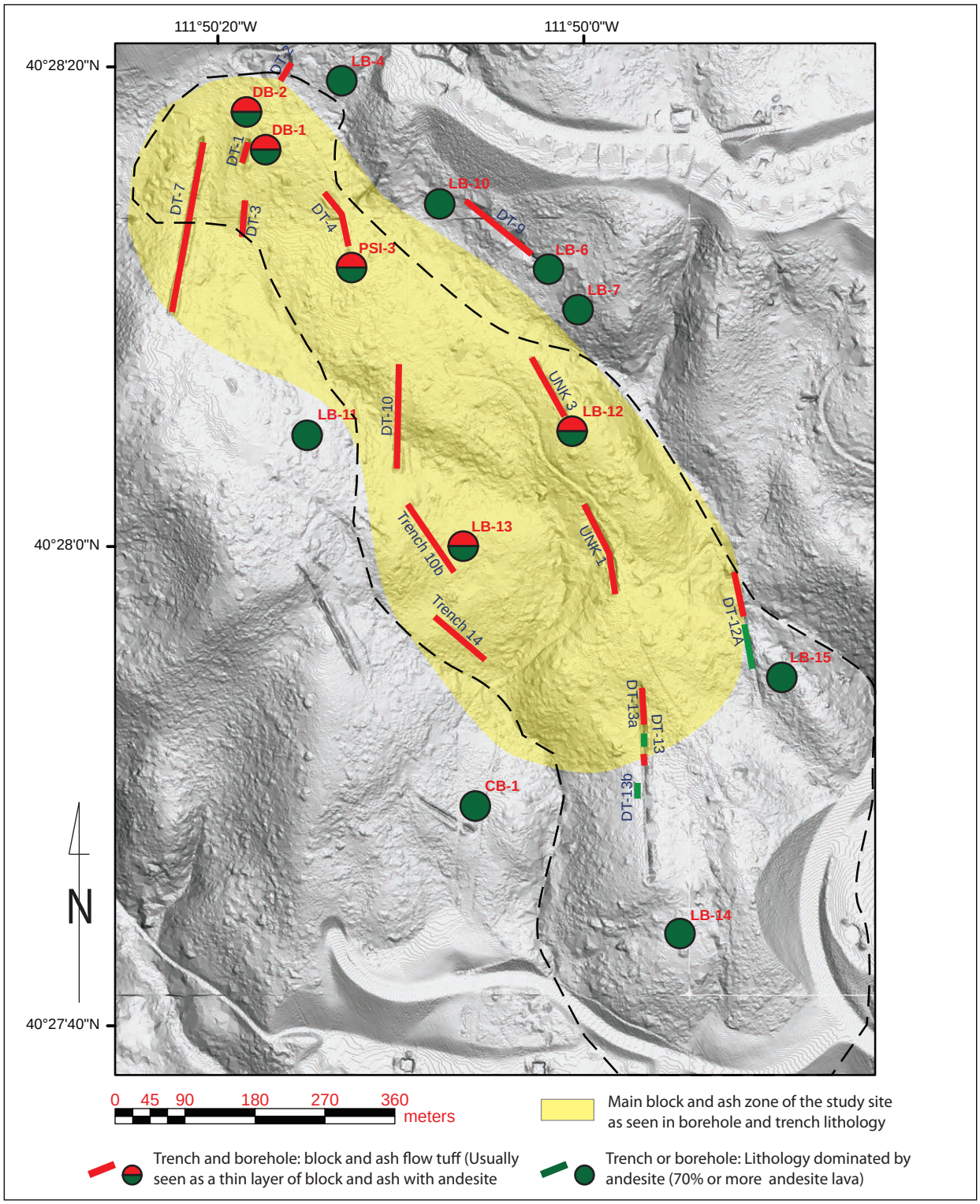

Figure 21 - *LiDAR map of the south slope, with borehole and trench locations showing rock type. Boreholes or trenches with about 70% or more of block and ash flow tuff or andesite lavas are colored green. Boreholes marked with both red and green signify boreholes found with a significant interval of block and ash flow tuffs above a basal interval of andesite lavas. The central zone of the study area contains a large body of block and ash flow volcanic rock, surrounded by the andesite lavas. The occurrence of block and ash flow tuffs correlates to the location of Biek's (2005a) possible mapped landslide unit shown by the dashed line.*

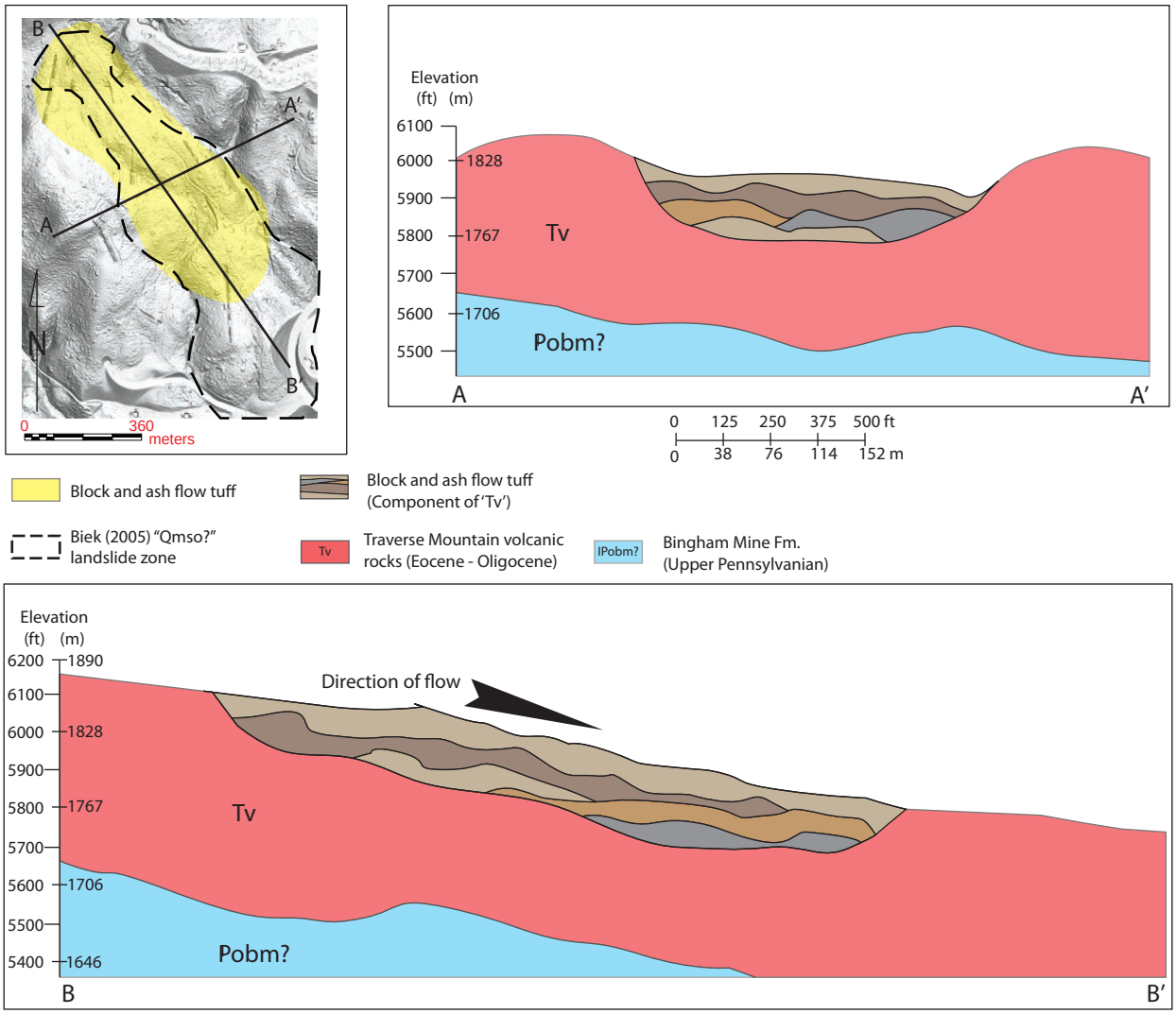

Figure 22 - *Cartoon cross section of the block and ash flow tuff interior. This figure does not represent actual boundaries or known block and ash flow tuff deposits, but shows a conceptual model of how they would appear if mappable. Based on the trench and borehole logs, the architecture is likely a chaotic series flows, which truncate and end abruptly against others within the study area. The tuffs appear to have flowed down slope to the south. (scale is 1:1)*

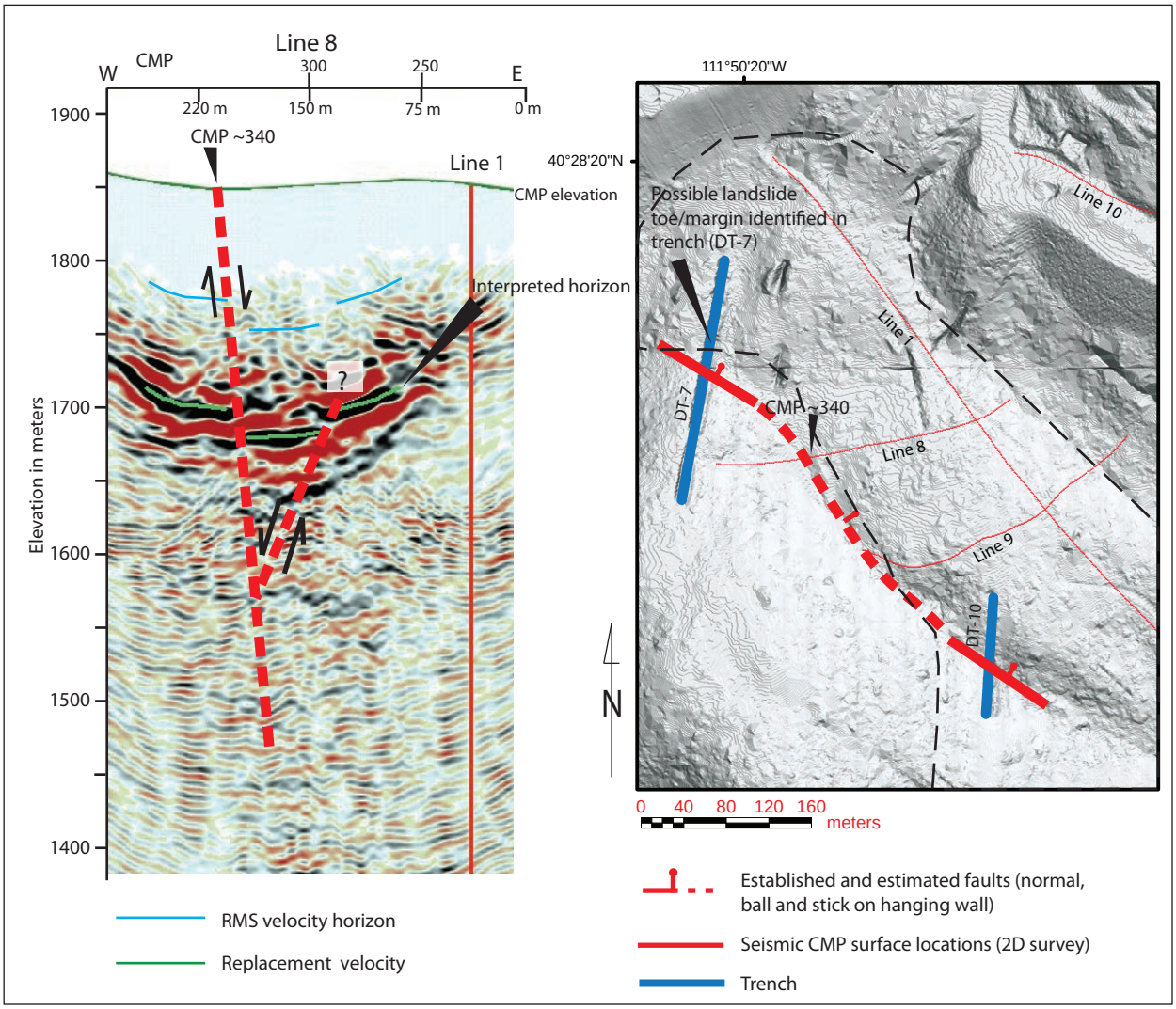

Figure 23 - *Seismic line 8 (left) and LiDAR hillshade surface map (right) showing the normal fault correlation discussed in the text. The interpreted horizon at depth (left) has a small graben-like depression which may be linked to the two normal faults identified in trenches DT-7 and DT-10 (hanging wall to the north-east). Dashed line shows Biek's (2005a) possible landslide unit.*